MNRAS **446,** 3651–3668 (2015) doi:10.1093/mnras/stu2337

New insights on Ba overabundance in open clusters.* Evidence for the intermediate neutron-capture process at play?

T. Mishenina,[1,2] M. Pignatari,[3]† G. Carraro,[4,5] V. Kovtyukh,[1,2]‡ L. Monaco,[4] S. Korotin,[1,2] E. Shereta,[1] I. Yegorova[4] and F. Herwig[6,7]†

[1]*Astronomical Observatory, Odessa National University, Shevchenko Park, UA-65014 Odessa, Ukraine*
[2]*Isaac Newton Institute of Chile, Odessa branch, Shevchenko Park, 65014 Odessa, Ukraine*
[3]*Department of Physics, University of Basel, Klingelbergstrabe 82, CH-4056 Basel, Switzerland*
[4]*European Southern Observatory, Alonso de Cordova 3107, 19001 Santiago de Chile, Chile*
[5]*Dipartimento di Fisica e Astronomia, Universitá di Padova, I-35122, Padova, Italy*
[6]*Department of Physics & Astronomy, University of Victoria, Victoria, BC V8P5C2, Canada*
[7]*Joint Institute for Nuclear Astrophysics, The Joint Institute for Nuclear Astrophysics, Notre Dame, IN 46556, USA*

Accepted 2014 November 3. Received 2014 November 2; in original form 2014 August 17

ABSTRACT

Recently, an increasing number of studies were devoted to measure the abundances of neutron-capture elements heavier than iron in stars belonging to Galactic Open Clusters (OCs). OCs span a sizeable range in metallicity ($-0.6 \leq$ [Fe/H] $\leq +0.4$), and they show abundances of light elements similar to disc stars of the same age. A different pattern is observed for heavy elements. A large scatter is observed for Ba, with most OCs showing [Ba/Fe] and [Ba/La] overabundant with respect to the Sun. The origin of this overabundance is not clearly understood. With the goal of providing new observational insights, we determined radial velocities, atmospheric parameters and chemical composition of 27 giant stars members of five OCs: Cr 110, Cr 261, NGC 2477, NGC 2506 and NGC 5822. We used high-resolution spectra obtained with the UVES spectrograph at European Southern Observatory Paranal. We perform a detailed spectroscopic analysis of these stars to measure the abundance of up to 22 elements per star. We study the dependence of element abundance on metallicity and age with unprecedented detail, complementing our analysis with data culled from the literature. We confirm the trend of Ba overabundance in OCs, and show its large dispersion for clusters younger than ∼4 Gyr. Finally, the implications of our results for stellar nucleosynthesis are discussed. We show in this work that the Ba enrichment compared to other neutron-capture elements in OCs cannot be explained by the contributions from the slow neutron-capture process and the rapid neutron-capture process. Instead, we argue that this anomalous signature can be explained by assuming an additional contribution by the intermediate neutron-capture process.

Key words: stars: abundances – stars: late-type – Galaxy: disc – Galaxy: evolution.

1 INTRODUCTION

In Mishenina et al. (2013a), we reported on the detailed chemical abundance analysis of giant stars in the open clusters (OCs) Ruprecht 4, Ruprecht 7, Berkeley 25, Berkeley 73, Berkeley 75, NGC 6192, NGC 6404, and NGC 6583. Our analysis was focused on neutron-capture elements located at the first and second neutron-magic peaks beyond iron ($N = 50$ and 82, respectively). In the Solar system, about half of the abundance beyond Fe are made by the slow neutron-capture process (*s*-process, e.g. Käppeler et al. 2011, and references therein), while the other half is made by the rapid neutron-capture process (*r*-process; e.g. Thielemann et al. 2011, and references therein). On average, most OCs have a metallicity around the Sun (with some exceptions), therefore any relevant departure from solar abundances of heavy elements provides important insights about OCs formation and about the production of these elements in stars. Using as a reference the Solar system, heavy elements that are mostly produced by the *s*-process are

* Based on observations collected at Paranal Observatory under programme 088.D-0045.

‡E-mail: val@deneb1.odessa.ua
†NuGrid Collaboration, http://www.nugridstars.org.

usually called *s*-process elements. Ba and La are typical examples of this group, located at the neutron shell closure $N = 82$. According to the residual method, heavy elements that instead are not produced efficiently by the *s*-process are *r*-process elements, e.g. Eu (e.g. Bisterzo et al. 2014). Galactic chemical evolution simulations have shown that starting from Ba and for heavier elements, the residual method provides results that are quite consistent with spectroscopic observations of old metal-poor *r*-process-rich stars (Travaglio et al. 2004). In this work, we will use the same naming scheme of *s*-process and *r*-process elements for OCs. Between the Sr neutron-magic peak and Xe, the residual method seems to fail to reproduce the Solar system inventory, requiring the introduction of an alternative nucleosynthesis component, called lighter element primary process, or LEPP (Travaglio et al. 2004). If this component is the same as observed in a sample of old metal-poor stars in the galactic halo is still a matter of debate (Montes et al. 2007). A larger amount of stellar data are becoming available in the last years for metal-poor stars, including abundances of elements in the mass region between Sr and Ba, e.g. Ag and Pd (e.g. Hansen et al. 2012). This will allow in the near future to better constrain the origin of the LEPP at low metallicity. Different nucleosynthesis processes have been proposed as a source of the LEPP, in the early Galaxy and eventually in the Solar system (Hoffman et al. 1996; Fröhlich et al. 2006; Pignatari et al. 2008; Qian & Wasserburg 2008; Farouqi et al. 2009; Arcones & Montes 2011; Frischknecht, Hirschi & Thielemann 2012). Recently, the existence of the LEPP for the Solar system has been questioned, and observations of heavy elements in OCs compared to the Sun were one of the main arguments used to support this analysis (Maiorca et al. 2012; Trippella et al. 2014).

Nevertheless, the peculiar high Ba abundance compared to Fe and other heavy elements with respect to the Sun observed in a number of OCs, remains a puzzle. From available data, Ba overabundance seems to be present at any age and metallicity, and seems to increase at decreasing age (Maiorca et al. 2011; D'Orazi et al. 2012; Yong, Carney & Friel 2012; Jacobson & Friel 2013; Mishenina et al. 2013a). The origin of this overabundance, however, is not understood, and the data analysis far from being homogeneous. One way to get more insight on this problem is to study the overabundance in a wider age and metal abundance range. To this aim, in this study, we add to the original Mishenina et al. (2013b) sample five more OCs: Cr 110, Cr 261, NGC 2477, NGC 2506, and NGC 5822, allowing us to cover within a consistent analysis a wider range in metallicity ($-0.2 \leq$ [Fe/H] $\leq +0.15$) and age (0.5 to 7.0 Gyr).

Previous studies are available for all these clusters, with partial overlap. In particular, three stars in Cr 110 were studied by Pancino et al. (2010), six stars in Cr 261 from Carretta et al. (2005), six stars in NGC 2477 from Bragaglia et al. (2008), four stars in NGC 2506 from Carretta et al. (2005), and, lastly, three stars in NGC 5822 from Santos et al. (2009). We anticipate that good agreement is in general obtained for all the stars in common. Some exceptions are present for Ba, where we found discrepancies up to 0.3 dex between different works for the [Ba/Fe], and 0.4 dex in one case.

Additionally, the same observational material presented here for NGC 2477 and NGC 5822, has also been recently analysed by Caffau et al. (2014, hereafter C14). The C14 study allows for an independent cross check on the atmospheric parameters and iron content derived for the programme stars and provide an assessment on the typical differences on these parameters as derived by different researchers even when adopting similar, although not identical techniques.

The data quality and origin, and the analysis techniques are identical to Mishenina et al. (2013b). In particular, non-local thermodynamic equilibrium (NLTE) conditions are adopted in deriving Ba abundance.

The layout of the paper is as follows. In Section 2, we describe how data were collected and reduced. Section 3 is devoted to the determination of the stars' photospheric parameters (effective temperature $T_{\rm eff}$, surface gravity log g, and microturbulence velocity $V_{\rm t}$), while Section 4 illustrates how we perform the abundance analysis. Our results, together with a comparison with literature material, are discussed in Section 5. Finally, in Section 6, we discuss our results in the framework of stellar nucleosynthesis. Conclusions and final remarks are given in Section 7.

2 OBSERVATIONS AND DATA REDUCTION

The main parameters: galactic coordinates (for J2000.0), galactocentric distance $R_{\rm GC}$, and age, of the investigated clusters are listed in the Table 1, together with the observation epochs and signal-to-noise (SNR) range. Age and distances are obtained from the sources listed in the last column. In particular, Galactocentric distances have been re-scaled to a Sun distance to the Galactic Centre of 8.5 kpc.

Observations were taken in service mode using the multi-object fibre-fed FLAMES facility mounted at the European Southern Observatory (ESO)-VLT/UT2 telescope at the Paranal Observatory (Chile). Two or three exposures (depending on the cluster, see Table 1) were taken with the red arm of the UVES high-resolution spectrograph. The UVES spectrograph was set up around a 5800 Å central wavelength, thus covering the 4760–6840 Å wavelength range and providing a resolution of $R \simeq 47\,000$.

Radial velocities (see Table 2) were computed using the IRAF/`fxcor` task to cross-correlate the observed spectra with a synthetic one from the Coelho et al. (2005) library with stellar parameters $T_{\rm eff} = 5250$ K, log $g = 2.5$, solar metallicity, and no α-enhancement. The IRAF `rvcorrect` task was used to calculate the correction from geocentric velocities to heliocentric.

We took the stars' radial velocity to be the average of the two/three epochs measured and the error (σ) to be the maximum deviation between the two/three values from the mean, multiplied by 0.63 (small sample statistics; see Keeping 1962).

Table 1. The main parameters of the investigated clusters. The last column indicates the source for age and distance.

Name	l (deg)	b (deg)	$R_{\rm GC}$ (kpc)	age (Gyr)	Exposure (s)	Date	SNR	
Collinder 110	209.649	−01.927	10.2	1.3	2 × 2000	Feb 28, Mar 06 (2012)	26–64	Bragaglia & Tosi (2003)
Collinder 261	301.684	−05.528	7.5	7.0	3 × 2400	Feb 24, Mar 01, 06 (2012)	39–53	Gozzoli et al. (1996)
NGC 2477	253.563	−05.838	8.9	0.6	3 × 1500	Oct 28 (2011), Mar 08 (2012)	66–92	D'Orazi et al. (2009)
NGC 2506	230.564	09.935	10.9	1.9	2 × 2000	Feb 03, Mar 07 (2012)	20–87	Reddy et al. (2012)
NGC 5822	321.577	03.585	7.9	0.45	3 × 1000	Mar 01, 06, 24 (2012)	92–108	Carraro et al. (2011)

Table 2. The main parameters of the investigated stars.

Name	RA(2000.0) (deg)	Dec(2000.0) (deg)	V (mag)	$B-V$ (mag)	$T_{\rm eff}$ (^{o}K)	log g	$V_{\rm t}$ (km s^{-1})	[Fe/H]	$V_{\rm r}$ (km s^{-1})	Membership
Cr 110										
1122	99.705 000	2.108 611	13.740	1.383	4954	2.6	1.2	− 0.05	38.19 ± 0.10	M
1134	99.687 500	2.073194	13.704	1.360	4940	2.6	1.2	0.02	38.14 ± 0.13	M
1149	99.712 917	2.065 083	13.637	1.389	4906	2.6	1.2	− 0.01	37.46 ± 0.39	M
1151	99.726 667	2.066 278	13.691	1.327	4956	2.6	1.2	0.02	37.94 ± 0.04	M
2129	99.671 250	2.018 139	13.656	1.340	4933	2.6	1.2	− 0.04	38.69 ± 0.11	M
3122	99.644 583	2.028 056	13.464	1.378	4758	2.4	1.0	− 0.03	39.94 ± 0.05	M
Cr 261										
2269	189.412 917	− 68.386 806	14.241	1.403	4575	2.4	1.2	− 0.02	− 28.03 ± 0.14	M
2291	189.480 417	− 68.413 861	13.572	1.328	4746	2.5	1.2	0.00	− 24.18 ± 0.14	M
2309	189.551 667	− 68.342 139	13.718	1.286	4746	2.5	1.2	0.00	− 26.23 ± 0.16	M
2311	189.545 000	− 68.392 778	14.164	1.362	4778	2.5	1.15	− 0.02	− 25.56 ± 0.15	M
2313	189.556 667	− 68.399 333	14.011	1.448	4674	2.5	1.2	− 0.01	− 23.20 ± 0.11	M
NGC 2477										
4027	118.087 917	− 38.577 194	12.153	1.198	4966	2.7	1.4	0.10	7.03 ± 0.13	M
4221	118.152 083	− 38.631 750	12.270	1.171	4975	2.8	1.2	0.19	8.80 ± 0.23	M
5043	118.040 417	− 38.598 306	12.165	1.170	5001	2.8	1.2	0.08	13.22 ± 0.27	NM
5076	118.061 667	− 38.629 194	12.410	1.220	4954	2.7	1.2	0.18	9.22 ± 0.33	M
7266	117.955 000	− 38.535 694	12.252	1.193	4966	2.8	1.2	0.19	9.30 ± 0.14	M
7273	117.947 917	− 38.543 389	12.390	1.174	4985	2.8	1.2	0.20	8.77 ± 0.51	M
8216	118.064 583	− 38.457 306	12.334	1.272	4945	2.7	1.2	0.14	3.99 ± 0.50	NM
NGC 2506										
1112	120.013 750	− 10.762 250	12.961	0.958	4969	2.6	1.2	− 0.22	83.99 ± 0.27	M
1229	120.030 833	− 10.740 722	13.118	1.011	4728	2.4	1.0	− 0.22	82.54 ± 0.58	M
2109	120.029 583	− 10.779 000	13.146	0.890	5040	2.6	0.9	− 0.22	89.31 ± 0.05	NM
2380	120.038 750	− 10.818 806	13.187	0.927	4992	2.6	1.0	− 0.19	83.64 ± 0.53	M
3231	119.982 917	− 10.805 944	13.105	0.952	4974	2.6	1.2	− 0.22	84.36 ± 0.51	M
5271	120.028 750	− 10.752 000	13.204	0.923	4993	2.6	1.15	− 0.24	83.52 ± 0.15	M
NGC 5822										
13292	226.164 167	− 54.351 139	10.401	1.040	5010	2.8	1.2	0.04	− 29.35 ± 0.34	M
16450	226.059 167	− 54.429 833	10.281	1.050	4972	2.6	1.2	− 0.02	− 25.69 ± 0.37	NM
18897	225.955 833	− 54.336 278	10.842	1.014	5030	2.7	1.0	− 0.02	− 29.01 ± 0.22	M
2397	226.071 250	− 54.473 111	10.455	1.010	5036	2.8	1.1	0.02	− 29.67 ± 0.79	M

Notes. The data of V and $B-V$ were taken from Bragaglia & Tosi (2003) for Cr 110, from Gozzoli et al. (1996) for Cr 261, from Kassis et al. (1997) for NGC 2477, from Marconi et al. (1997) for NGC 2506, and from Carraro et al. (2011) for NGC 5822.

Membership assessment was performed by looking at the radial velocity distribution only, and assigning individual star membership to a cluster when the star radial velocity is within 2σ from the cluster mean radial velocity. By adopting this criterion, stars are classified as members (M) or not members (NM) in the last column of Table 2. In most cases, we found that the observed giants were cluster members.

We compared the stars radial velocity with the literature, and found the following:

Collinder 110: Pancino et al. (2010) report 38.74 ± 0.64 km s^{-1} for star #2129, which is very close to our estimate (see Table 2). The lower resolution study by Carrera et al. (2007) suggest a mean cluster velocity of 45 ± 8 km s^{-1} from eight stars. This value is again in fine agreement with Pancino et al. (2010) and this study.

NGC 2506: star #3231 was measured by Reddy, Giridhar & Lambert (2012). Their value (84.9 ± 0.4km s^{-1}) is in fine agreement with ours. Besides, except for star #5271, all our programme stars have measurements in Mermilliod, Mayor & Udry (2008). Our values are in fine agreement for all the common stars. In particular, star #2109, that we considered a non-member, has a very different radial velocity in Mermilliod et al. (2008). Its velocity (80.92 km s^{-1}) confirms it is most probably a binary star.

Collinder 261: we do not have any star in common with Carretta et al. (2005), however our radial velocities are fully compatible with that study. # 2291 and 2311 are in common with De Silva et al. (2007), and their values (−27.8 and −18.1) are only in marginal agreement with our study. De Silva et al. (2007) are, however, based only on a narrow spectral range, and are affected by errors as a large as 2 km s^{-1}.

NGC 2477: Mermilliod et al. (2008) measured radial velocity for 83 stars in NGC 2477. They obtained 7.26 ± 1.00 km s^{-1} as cluster mean radial velocity. Our programme stars have compatible radial velocity, and support the non-member nature of stars # 5043 and 8216.

NGC 5822: the most recent radial velocity study is from Mermilliod et al. (2008). These authors derive a mean radial velocity of −29.31 ± 0.82 km s^{-1} from 28 stars, and this is in nice agreement with our values. This confirms our classification as non-member of star #16450.

In conclusion, the agreement with literature values is in general very good.

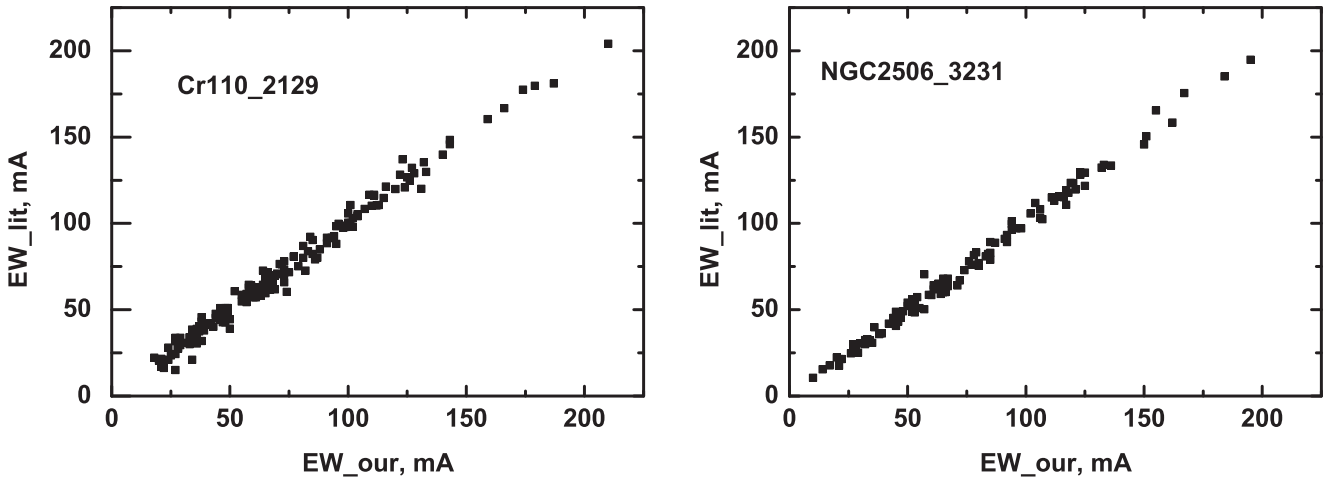

Figure 1. The comparison of the EW for star Cr 110_2129 and NGC 2506_3231 with literature data.

The processing of spectra (continuum definition, equivalent widths (EW) measurements etc.) was carried out using the DECH20 software package (Galazutdinov 1992). The results of the comparison of the EW of the lines measured in this work with the ones measured by other authors for two giant stars are the following: Cr 110 (star 2129, Pancino et al. 2010), (EW(our) – EW(lit)) = 0.11 ± 4.44 mÅ (162 lines) and NGC 2506 (star 3231, Reddy et al. 2012), (EW(our) − EW(lit)) = 0.05 ± 3.64 mÅ (116 lines). This is illustrated in the panels of Fig. 1, from which one can appreciate the good agreement between the different measurement systems.

3 STELLAR ATMOSPHERIC PARAMETERS

Stars' effective temperatures $T_{\rm eff}$ were estimated by calibrating the ratio of the central depths of the lines with different potentials of the lower levels developed by Kovtyukh et al. (2006). The surface gravities log g were computed using the iron ionization balance. The microturbulence velocity Vt was derived considering that the iron abundance log A(Fe) obtained from the given Fe I line is not correlated with the EW of that line. The adopted value of the metallicity [Fe/H] is calculated using the iron abundance obtained from Fe I lines. The resulting atmospheric parameters are presented in Table 2.

The comparison of the atmospheric parameters with literature data is presented in Table 3. One can notice that the external accuracy of the effective temperature $T_{\rm eff}$ is within $\Delta T_{\rm eff} = \pm 100$ K, the surface gravity log g – Δlog g= ±0.2 dex, except the star Cr 261_2311. The difference in $T_{\rm eff}$ for this star reaches 178 K, and 0.5 for gravity. To check the choice of the temperatures, we investigated dependences of iron abundances log A(Fe I) determined using the Fe I lines on its excitation potential of low level and on EW for two microturbulence velocities and for two models with $T_{\rm eff} = 4748$ K (our determination) and $T_{\rm eff} = 4600$ K (De Silva et al. 2007). This is shown in the panels of Fig. 2, from which one can appreciate the lack of any clear trend.

The comparison with the C14 study for the stars observed in NGC 2477 and NGC 5822 is presented in the second part of Table 3. The agreement is generally good, with a maximum difference in $T_{\rm eff}$ and log g of 109 K and 0.3 dex, for star #2397 and #18897 in NGC 5822, respectively. We derive an iron content on average ∼0.04 and ∼0.12 dex higher than C14, for stars in NGC 5822 and NGC 2477, respectively. The maximum differences are noted for NGC 2477 stars #4221 (0.16 dex), #5076 (0.16 dex), and #7273

Table 3. Comparison of atmospheric parameters.

Star	$T_{\rm eff}$, K	log g (lit.)	$V_{\rm t}$	[Fe/H]	$T_{\rm eff}$, K	log g (this study)	$V_{\rm t}$	[Fe/H]
Cr 110 2129 (Pancino et al. 2010)	4950	2.7	1.4	0.05	4933	2.6	1.2	−0.04
NGC 2506 (Reddy et al. 2012)	5000	2.5	1.4	−0.25	4974	2.6	1.2	−0.22
	$T_{\rm eff}$, K	log g	$V_{\rm t}$	log A(Fe)	$T_{\rm eff}$, K	log g	$V_{\rm t}$	log A(Fe)
Cr 261 2291 (De Silva et al. 2007)	4650	2.3	1.8	7.51	4746	2.5	1.2	7.57
Cr 261 2311 (De Silva et al. 2007)	4600	2.0	0.9	7.56	4778	2.5	1.15	7.55
NGC 2477 4027 (C14)	4998	2.78	1.12	7.66	4966	2.7	1.4	7.67
NGC 2477 4221 (C14)	4956	2.70	1.12	7.60	4975	2.8	1.2	7.76
NGC 2477 5043 (C14)	5075	2.96	1.06	7.56	5001	2.8	1.2	7.65
NGC 2477 5076 (C14)	5010	2.80	1.14	7.59	4954	2.7	1.2	7.75
NGC 2477 7266 (C14)	5036	2.92	1.09	7.65	4966	2.8	1.2	7.76
NGC 2477 7273 (C14)	4977	2.67	1.20	7.54	4985	2.8	1.2	7.77
NGC 2477 8216 (C14)	5017	2.84	0.99	7.64	4945	2.7	1.2	7.71
NGC 5822 13292 (C14)	5066	2.80	1.12	7.57	5010	2.8	1.2	7.61
NGC 5822 16450 (C14)	5017	2.71	1.09	7.51	4972	2.6	1.2	7.55
NGC 5822 18897 (C14)	5115	3.00	1.10	7.50	5030	2.7	1.0	7.55
NGC 5822 2397 (C14)	5145	2.95	1.13	7.57	5036	2.8	1.1	7.59

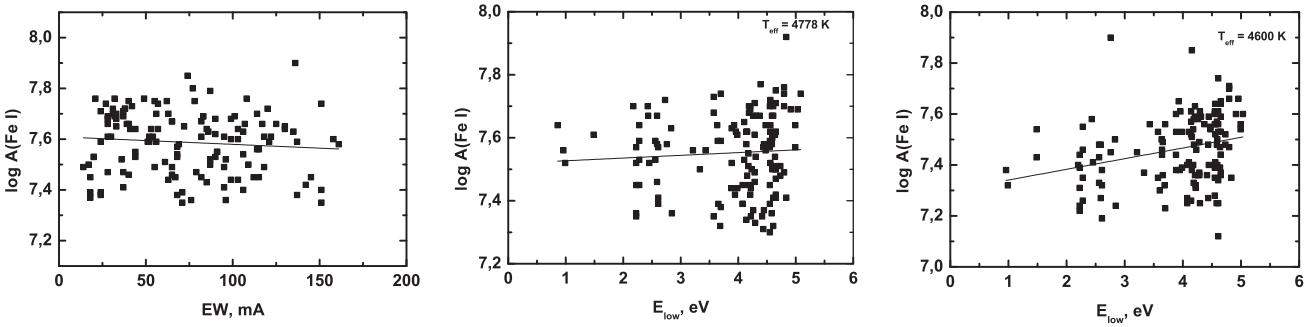

Figure 2. For star Cr 261_2311, the dependence of the iron abundance (based on Fe I lines) on the EW (choice of turbulent velocity V_t, left) and a similar dependence of the iron abundance on the potential of the lower level of the line E_{low} for two values of the effective temperature T_{eff} (middle and right).

(0.23 dex), C14 adopted a solar iron abundance of 7.52, compared to the 7.57 adopted here. For the sake of an easier comparison, we reported absolute iron abundances in Table 3. Several authors have investigated in the literature differences in the derived abundances and chemical parameters as estimated by different researchers adopting different prescriptions and approaches (see, e.g. Bensby et al. 2009; Gilmore et al. 2013). We consider the agreement with C14 analysis as satisfactory. It provides as well an estimate of the differences which one expects from the analysis performed by different authors. Note that the mentioned differences are not affecting the results of this work.

4 ABUNDANCE ANALYSIS

The abundances of the investigated elements are determined for 27 giants using the local thermodynamic equilibrium (LTE) approximation, and atmosphere models by Castelli & Kurucz (2004), computed for the parameters of each star. The estimate of the oxygen and Eu abundance was performed with a new version of the STARSP software package (Tsymbal 1996). For this, we used the line list in the region of the [O I] line 6300.3 Å and the europium line 6645.13 Å from the VALD atomic data (Kupka et al. 1999).

The magnesium, sodium, and barium abundances were computed in NLTE approximation with a version of MULTI (Carlsson 1986), modified by S. Korotin (Korotin & Mishenina 1999; Mishenina et al. 2004; Korotin et al. 2011). We used the Mg I lines 5172.69, 5183.61, 5528.41, 5711.09, 6318.7, 6319,24, 6319.49 ÅÅ; the Na I 5682.65, 5688.22, 6154.23, 6160.75 ÅÅ, and three lines of Ba II(5853, 6141, and 6496 ÅÅ).

The model of sodium atom consists of 27 levels of Na I and the ground level of Na I. We considered the radiative transitions between the first 20 levels of Na I and the ground level of Na II. Transitions between the remaining levels were used only in the equations of particle number conservation. Finally, 46 $b-b$ and 20 $b-f$ transitions were included in the linearization procedure. The NLTE corrections for the Na abundances are $\lesssim$0.2 dex.

We employed the model of magnesium atom consisting of 97 levels: 84 levels of Mg I, 12 levels of Mg II, and a ground state of Mg III. Within the described system of the magnesium atom levels, we considered the radiative transitions between the first 59 levels of Mg I and ground level of Mg II. Transitions between the rest levels were not taken into account and they were used only in the equations of particle number conservation. The NLTE corrections for the Mg abundances are $\lesssim$0.1 dex. Our Ba model contains 31 levels of Ba I, 101 levels of Ba II with $n < 50$, and the ground level of Ba III ion. We also included 91 bound–bound transitions. The odd Ba isotopes have hyperfine splitting of their levels and, thus, several hyperfine structure (HFS) components for each line (Rutten 1978). Therefore, line 6496 Å was fitted by adopting the even-to-odd abundance ratio of 82:18 (Cameron 1982). The HFS for lines 5853 Å and 6141 Å is not significant. The solar Ba abundance was assumed to be $(Ba/H)_\odot = 2.17$ where $\log A(H) = 12$. That value was obtained from the Solar Atlas (Kurucz et al. 1984) with the same atomic data, which had been used to estimate the Ba abundance in the stellar atmospheres. The influence of the NLTE does not have any significant effect in the examined stars. The NLTE corrections for the Ba abundances are $\lesssim$0.1 dex.

4.1 Errors in abundance determinations

The effects of uncertainties in atmospheric parameters on the accuracy of elemental abundance determinations for star NGC 2477_7266 is given in Table 4. The typical errors in temperature T_{eff}, surface gravity $\log g$ and microturbulent velocity V_t are ±100 K (col 1), ±0.2 (col 2), and ±0.2 km s^{-1} (col 3), respectively. The total error (col 4) includes the mean error in the EW

Table 4. Abundance uncertainties due to atmospheric parameters. NGC 2477_7266 (T_{eff} = 4966, $\log g$ = 2.8, V_t = 1.2, [Fe/H] = 0.19).

Species	Δ T_{eff}+100	Δ $\log g$+0.2	Δ V_t+0.02	Total
O I	0.02	0.08	0.00	0.09
Na I	0.08	0.01	0.02	0.10
Mg I	0.05	0.01	0.04	0.08
Al I	0.07	0.01	0.03	0.09
Si I	0.02	0.01	0.03	0.06
Ca I	0.09	0.03	0.09	0.14
Sc II	0.01	0.07	0.05	0.10
Ti I	0.13	0.01	0.04	0.14
Ti II	0.01	0.07	0.07	0.11
V I	0.14	0.00	0.05	0.16
Cr I	0.09	0.01	0.05	0.11
Fe I	0.07	0.01	0.07	0.11
Fe II	0.08	0.06	0.07	0.13
Co I	0.07	0.03	0.04	0.10
Ni I	0.05	0.02	0.05	0.09
Y II	0.00	0.07	0.10	0.13
Zr II	0.01	0.08	0.02	0.10
Ba II	0.02	0.03	0.14	0.16
La II	0.02	0.08	0.05	0.11
Ce II	0.01	0.08	0.01	0.10
Nd II	0.01	0.08	0.04	0.10
Eu II	0.01	0.07	0.04	0.10

Table 5. Solar abundance derived by us and compared with photospheric abundance by Asplund et al. (2009).

Species	log *A* (this work)	NL	Asplund et al. (2009)
O I	**8.70**	1	8.69 ± 0.05
Na I	**6.25 ± 0.04**	10	6.24 ± 0.04
Mg I	**7.58 ± 0.02**	9	7.60 ± 0.04
Al I	6.30 ± 0.01	2	6.45 ± 0.03
Si I	7.55 ± 0.08	23	7.51 ± 0.03
Ca I	6.32 ± 0.07	16	6.34 ± 0.04
Sc I	–		3.15 ± 0.04
Sc II	3.22 ± 0.11	14	–
Ti I	4.96 ± 0.08	41	4.95 ± 0.05
Ti II	5.01 ± 0.03	5	–
V I	4.04 ± 0.12	36	3.93 ± 0.08
Cr I	5.67 ± 0.09	23	5.64 ± 0.04
Fe I	7.57 ± 0.08	164	7.50 ± 0.04
Fe II	7.47 ± 0.04	11	–
Co I	5.00 ± 0.10	28	4.99 ± 0.07
Ni I	6.29 ± 0.06	56	6.22 ± 0.04
Y II	2.15 ± 0.17	7	2.21 ± 0.05
Zr I	–		2.58 ± 0.04
Zr II	2.79 ± 0.19	2	–
Ba II	**2.17 ± 0.04**	4	2.18 ± 0.09
La II	1.24 ± 0.02	2	1.10 ± 0.04
Ce II	1.70 ± 0.11	6	1.58 ± 0.04
Nd II	1.54 ± 0.08	11	1.42 ± 0.04
Eu II	**0.60**	1	0.52 ± 0.04

Notes. The abundance values computed with synthetic spectrum marked as bold.

measurements and the accuracy of the synthetic spectrum fitting that is assumed to be 0.05 dex.

As can be seen from Table 4, the total error in the elemental abundance determinations is less than 0.2 dex. In particular, the error associated with the determination of the Ba abundances is 0.16 dex.

The solar abundance computed for the lines from the Solar spectrum (Kurucz et al. 1984) with log *gf* from VALD data base (Kupka et al. 1999) and the solar model (Castelli & Kurucz 2004) is given in Table 5. The elemental abundances obtained by us for studied OCs, namely Cr 110, Cr 261, NGC 2477, NGC 2506, and NGC 5822 are given in Tables 6–10 and the mean abundance values for each cluster are presented in Table 11.

Since the Ba overabundance found for a number of OCs is the most controversial result from recent spectroscopic observations of OCs, here below we discuss possible source of uncertainties that may affect Ba measurements. In particular, let us consider possible causes of the Ba overabundance resulted from the EW measurements, applying methods of abundance determination, such as growth curve or synthetic spectrum techniques under both the LTE and non-LTE approximations, usage of different atmospheric model grids, etc.

The investigated Ba II lines (4554, 5853, 6141, and 6496 ÅÅ) tend to be strong (ranging from 100 to 450 mÅ) in the spectra of OC giants. In this case, it is crucial to correctly account for the wings of spectral lines, i.e. to establish the continuous spectrum level. That may cause errors in the EW measurements of up to 10–15 per cent. It is especially important when measuring the EW of lines or when applying the growth-curve technique. Moreover, improper consideration of spectral line damping constants, especially the van der Waals broadening, can result in additional error. However, as the Ba lines are wide enough, their profiles are affected by blending of other lines. The 6141 Å line blending affects the central part of the line (Fe I line). The effects of such distortions (blending) in spectral line profiles can be taken into account only when calculating the synthetic spectrum.

The estimates obtained in the study by Mishenina et al. (2013a, figs 5 and 6 from that paper) indicate that the EW and profiles are rather sensitive to the Ba abundance. Relatively weaker and moderate lines (up to 200 mÅ) are very sensitive to the elemental abundance changes; whereas stronger lines when using the computed synthetic spectra, allow us to obtain the abundance values with an accuracy of not less than ±0.1 dex (see Figs 6 and 7). Applying different atmospheric model grids can also cause some uncertainty in the abundance determinations of up to 0.05–0.1 dex.

In the paper D'Orazi et al. (2012), the authors suggest several possible explanations for the Ba overabundance, such as: (1) neglecting the HFS of the Ba lines; (2) deviations from the LTE conditions; (3) the chromospheric activity (see also D'Orazi et al. 2009).

In the OCs studied by Mishenina et al. (2013a) and in this work, the Ba lines are strong and broad. Therefore, neglecting of the HFS is not relevant in this case. Concerning the second point mentioned by D'Orazi et al. (2012), we considered NLTE correction for the Ba analysis. Note also that LTE deviations that we found do not exceed 0.1 dex. Finally, concerning the chromospheric activity, already D'Orazi et al. (2012) did not find any correlation between the Ba abundance and the chromospheric activity indices for the investigated stars. We would therefore consider the impact of this last source of uncertainty as marginal.

Thus, the definition of the continuous spectrum level, the EW measurement errors, the usage different abundance determination techniques, the adoption of atomic parameters (damping constants), and various atmospheric models can result in uncertainties in Ba abundance estimates obtained by different authors of up to ∼0.2 dex.

However, we did find variations up to 0.3 dex between different references in the literature, and in one case almost 0.4 dex (see Section 5).

5 RESULTS AND COMPARISON WITH THE LITERATURE

The chemical composition for our programme clusters was the subject of several studies in the past. The purpose of this study, however, is mostly to analyse the behaviour of the neutron-capture elements. Here, we summarize previous measurements and compare with our results. A detailed comparison between this work and the literature is given in Table 15.

Collinder 110. This cluster has significant reddening ($E(B-V) = 0.54 \pm 0.03$ (Pancino et al. 2010). Pancino et al. (2010) obtained accurate abundances of 17 elements, included Y, Ba, La, and Nd. With a cluster metallicity [Fe/H] = +0.03 ± 0.10, they found a significant barium overabundance ([Ba/Fe] = 0.49 ± 0.06), and excess of neodymium [Nd/Fe] = 0.23 ± 0.20. The values of the yttrium [Y/Fe] = −0.10 ± 0.12 and lanthanum [La/Fe] = +0.03 ± 0.18 are instead close to solar.

We obtained the mean values of [Fe/H] = −0.02, a moderate excess of [Ba/Fe] = 0.34 and a slight excess of [Y/Fe] = 0.08 and [La/Fe] = 0.16.

Collinder 261. The reddening of this cluster has been derived several times: $E(B-V)$ is about 0.22 (the value is quite

Table 6. Abundance results for Cr 110.

	1122			1134			1149			1151			2129			3132		
Ion	[El/H]	σ	NL	[El/H]	σ	NL	[El/H]	σ	NL	[El/H]	σ	NL	[El/H]	σ	NL	[El/H]	σ	NL
O I	**0**	–	1	**0**	–	1	**0**	–	1	**0**	–	1	**0**	–	1	**−0**	–	1
Na I	**−0**	–	4	**−0**	–	4	**0**	–	4	**0**	–	4	**−0**	–	4	**−0**	–	4
Mg I	**−0**	–	7	**−0**	–	7	**−0**	–	7	**−0**	–	7	**−0**	–	7	**−0**	–	7
Al I	−0.06	0.01	2	0.05	0.06	2	−0.02	0.05	2	0.06	0.04	2	0.10	0.05	2	0.09	0.02	2
Si I	−0.02	0.09	14	0.04	0.11	17	0.06	0.16	21	0.08	0.13	18	0.00	0.13	17	0.00	0.11	20
Ca I	−0.04	0.08	11	0.04	0.14	11	−0.05	0.14	13	0.07	0.12	12	−0.06	0.11	12	−0.07	0.08	14
Sc II	−0.07	0.17	9	0.08	0.14	7	0.00	0.18	10	0.01	0.14	9	−0.09	0.07	8	−0.07	0.13	10
Ti I	−0.05	0.09	26	−0.04	0.10	31	−0.06	0.08	34	−0.01	0.10	34	−0.04	0.08	25	−0.04	0.12	30
Ti II	−0.06	0.10	4	−0.05	0.08	3	0.02	0.13	5	0.06	0.10	4	−0.09	0.14	4	0.08	0.11	4
V I	−0.07	0.08	15	−0.00	0.09	15	−0.07	0.08	20	−0.05	0.10	28	−0.03	0.09	19	−0.05	0.13	28
Cr I	−0.06	0.07	12	0.00	0.14	18	−0.09	0.09	8	0.07	0.10	15	−0.01	0.06	7	−0.05	0.04	10
Fe I	−0.06	0.11	112	0.02	0.12	120	−0.01	0.12	136	0.02	0.11	130	−0.04	0.09	119	−0.03	0.12	134
Fe II	−0.11	0.05	7	−0.07	0.07	8	−0.10	0.14	11	−0.11	0.11	8	−0.07	0.07	7	−0.13	0.10	8
Co I	−0.02	0.04	12	−0.03	0.10	23	−0.10	0.07	18	−0.05	0.12	21	−0.05	0.10	13	−0.07	0.10	16
Ni I	−0.06	0.08	30	−0.04	0.09	39	−0.08	0.10	45	−0.02	0.11	45	−0.09	0.07	37	−0.07	0.13	47
Y II	−0.04	0.15	8	−0.00	0.14	7	0.11	0.12	8	0.17	0.04	7	0.01	0.14	8	0.10	0.14	6
Zr II	−0.06	0.01	3	0.14	0.25	3	0.10	0.15	3	0.11	0.03	3	−0.09	0.18	3	0.00	0.15	3
Ba II	**0**	–	3	**0**	–	3	**0**	–	3	**0**	–	3	**0**	–	31	**0**	–	3
La II	0.09	0.08	2	0.07	0.02	2	0.19	0.06	2	0.19	0.13	3	0.10	0.05	3	0.24	0.10	2
Ce II	0.07	0.16	6	0.21	0.16	5	0.22	0.14	7	0.06	0.16	4	0.09	0.09	3	0.02	0.12	6
Nd II	0.09	0.14	10	0.16	0.11	6	0.14	0.10	9	0.08	0.11	8	0.03	0.11	9	0.02	0.07	9
Eu II	**0**	–	1	**0**	–	1	**0**	–	1	**0**	–	1	**0**	–	1	**0**	–	1

Notes. The abundance values computed with synthetic spectrum marked as bold.

Table 7. Abundance results of Cr 261.

	2269			2291			2309			2311			2313		
Ion	[El/H]	σ	NL	[El/H]	σ	NL	[El/H]	σ	NL	[El/H]	σ	NL	[El/H]	σ	NL
Na I	**0**	–	4	**0**	–	4	**0**	–	4	**0**	–	4	**0**	–	4
Mg I	**0**	–	7	**0**	–	7	**−0**	–	7	**0**	–	7	**0**	–	7
Al I	0.07	0.10	2	0.15	0.01	2	−0.01	0.13	2	0.10	0.11	2	0.18	0.11	2
Si I	0.07	0.13	15	0.05	0.12	19	0.08	0.13	16	0.05	0.11	17	0.03	0.14	18
Ca I	0.04	0.08	14	−0.09	0.11	9	−0.03	0.12	14	0.00	0.13	13	−0.09	0.12	11
Sc II	0.06	0.14	11	0.10	0.14	9	0.10	0.06	6	0.06	0.11	13	0.10	0.12	8
Ti I	0.06	0.13	44	0.05	0.14	41	0.03	0.15	40	0.03	0.10	40	0.01	0.13	39
Ti II	0.07	0.06	4	0.09	0.06	4	0.08	0.07	4	0.01	0.09	4	0.09	0.06	3
V I	0.14	0.10	21	0.10	0.13	27	0.06	0.12	30	0.05	0.12	28	0.14	0.14	26
Cr I	0.06	0.08	19	−0.00	0.11	14	−0.01	0.12	15	0.06	0.13	14	−0.06	0.08	14
Fe I	−0.02	0.11	116	0.00	0.11	133	0.00	0.12	135	−0.02	0.12	135	−0.01	0.11	106
Fe II	−0.08	0.15	7	−0.04	0.08	12	−0.07	0.09	8	−0.09	0.10	10	−0.08	0.07	9
Co I	0.03	0.12	16	0.01	0.16	17	0.05	0.17	19	0.02	0.14	20	0.05	0.18	21
Ni I	0.03	0.11	47	0.02	0.08	45	0.03	0.13	51	0.08	0.11	52	0.04	0.13	50
Y II	0.09	0.18	6	0.04	0.18	6	0.11	0.15	7	0.05	0.19	7	0.06	0.18	3
Zr II	0.01	0.16	3	0.03	0.10	3	0.13	0.04	2	0.08	0.10	2	0.11	0.22	2
Ba II	**0**	–	3	**0**	–	3	**0**	–	3	**0**	–	3	**0**	–	3
La II	0.12	0.01	2	0.11	0.07	4	0.18	0.02	2	0.15	0.09	2	0.18	0.11	2
Ce II	0.01	0.08	4	0.05	0.19	7	-0.00	0.16	6	0.05	0.17	8	0.14	0.18	8
Nd II	0.05	0.16	9	0.07	0.16	9	0.02	0.11	10	0.10	0.12	8	0.08	0.16	11
Eu II	**0**	–	1	**0**	–	1	**0**	–	1	**0**	–	1	**0**	–	1

Notes. The abundance values computed with synthetic spectrum marked as bold.

uncertain, (Mazur, Krzeminski & Kaluzny 1995), 0.33 (Janes & Phelps 1994), 0.25–0.34 (Gozzoli et al. 1996). The same is true for its chemical composition, which, however, shows significant study-to-study variations: [Fe/H] = −0.16 (Friel et al. 2002), −0.22 (Friel et al. 2003), −0.03 (Carretta et al. 2005), −0.03 (De Silva et al. 2007), +0.13 (Sestito et al. 2008), 0.00 (Mikolaitis et al. 2012). Concerning neutron-capture elements, a moderate excess of barium [Ba/Fe] = 0.30 ± 0.08 was found by Carretta et al. (2005), while a sub-solar value of [Zr/Fe] = 0.12 and [Ba/Fe] = 0.03 with an intrinsic scatter smaller than 0.05 dex were derived by De Silva et al. (2007).

These results are consistent with Carretta et al. (2005), while there is a discrepancy of about 0.3 dex with the [Ba/Fe] calculated by De Silva et al. (2007). [Y/Fe] = −0.21 ± 0.07 was found by Maiorca et al. (2011).

We derived a mean values of [Fe/H] = −0.01, a moderate excess of [Ba/Fe] = 0.33, and a slight excess of [Y/Fe] = 0.07 and [La/Fe] = +0.13.

Table 8. Abundance results for NGC 2477.

	4027		4221		5043		5076		7266		7273		8216	
Ion	[El/H]	σ, NL	[El/H]	σ, NL	[El/H]	σ, NL	[El/H]	σ, NL	[El/H]	σ, NL	[El/H]	σ, NL	[El/H]	σ, NL
O I	**−0**	– (1)	**−0.15**	– (1)	**−0.15**	– (1)	**−0.15**	– (1)	**−0.15**	– (1)	**−0.15**	– (1)	**−0.15**	– (1)
Na I	**0**	– (4)	**0.13**	– (4)	**0.06**	– (4)	**0.10**	– (4)	**0.12**	– (4)	**0.14**	– (4)	**0.09**	– (4)
Mg I	**−0**	– (7)7	**−0.02**	– (7)	**−0.09**	– (7)	**−0.01**	– (7)	**−0.01**	– (7)	**−0.06**	– (7)	**−0.10**	– (7)
Al I	0.00	0.12 (2)	−0.12	0.13(2)	−0.19	0.07(2)	−0.07	0.01(2)	−0.11	0.08(2)	-0.09	0.08(2)	−0.10	0.01(2)
Si I	0.07	0.17(21)	0.18	0.15(23)	0.09	0.16(23)	0.17	0.15(24)	0.20	0.17(23)	0.20	0.17(23)	0.16	0.20(21)
Ca I	0.00	0.10(11)	0.08	0.19(16)	0.00	0.10(16)	0.06	0.17(15)	0.09	0.11(16)	0.09	0.10(16)	0.07	0.11(14)
Ti I	− 0.04	0.06(22)	0.02	0.09(3)	−0.09	0.07(26)	−0.03	0.08(38)	0.02	0.09(30)	0.02	0.10(34)	−0.07	0.09(33)
Ti II	0.03	0.11 (4)	−0.03	0.09(3)	0.07	0.14(5)	0.19	0.18(5)	0.13	0.18(5)	0.16	0.17(5)	0.14	0.21(5)
V I	0.01	0.12(30)	0.11	0.14(34)	−0.06	0.10(32)	0.08	0.13(31)	0.05	0.13(32)	0.08	0.13(32)	−0.01	0.14(33)
Cr I	− 0.01	0.19(17)	0.07	0.14(19)	0.00	0.13(17)	0.01	0.09(16)	0.05	0.08(16)	0.07	0.08(16)	0.05	0.12(17)
Fe I	0.10	0.12(127)	0.19	0.09(122)	0.08	0.12(134)	0.18	0.12(145)	0.19	0.12(146)	0.20	0.10(130)	0.14	0.12(138)
Fe II	0.05	0.17 (8)	0.16	0.10(9)	0.07	0.05(10)	0.11	0.10(11)	0.17	0.18(9)	0.18	0.18(9)	0.12	0.06(10)
Co I	0.11	0.11(13)	0.15	0.13(18)	0.03	0.07(18)	0.14	0.12(19)	0.15	0.11(19)	0.16	0.10(17)	0.08	0.11(18)
Ni I	0.06	0.11(45)	0.15	0.10(49)	0.02	0.10(54)	0.12	0.10(47)	0.16	0.09(43)	0.17	0.11(5)	0.08	0.06(44)
Y II	0.17	0.09 (3)	0.06	0.12(4)	0.10	0.15(5)	0.15	0.17(5)	0.07	0.18(5)	0.10	0.18(5)	0.15	0.13(5)
Zr II	0.03	– (1)	0.10	0.19(2)	0.20	– (1)	0.20	0.18(2)	0.18	– (1)	0.22	– (1)	0.27	0.18(2)
Ba II	**0**	– (3)	**0.39**	– (3)	**0.39**	– (3)	**0.30**	– (3)	**0.30**	– (3)	**0.26**	– (3)	**0.29**	– (3)
La II	0.09	– (1)	0.30	0.08(2)	0.20	0.14(2)	0.22	– (1)	0.28	– (1)	0.20	– (1)	0.19	0.20(2)
Ce II	0.11	0.14 (4)	0.26	0.17(4)	0.26	0.14(6)	0.22	0.13(5)	0.10	0.18(5)	0.14	0.18(5)	0.22	0.09(5)
Nd II	0.06	0.11 (3)	0.00	0.01(2)	0.07	0.16(9)	0.04	0.16(8)	0.01	0.17(9)	0.18	0.18(9)	0.00	0.20(2)
Eu II	**0**	– (1)	**0.15**	– (1)	**0.15**	– (1)	**0.15**	– (1)	**0.18**	– (1)	**0.15**	– (1)	**0.25**	– (1)

Notes. The abundance values computed with synthetic spectrum marked as bold.

Table 9. Abundance results for NGC 2506.

	1112			1229			2109			2380			3231			5271		
Ion	[El/H]	σ	NL	[El/H]	σ	NL	[El/H]	σ	NL	[El/H]	σ	NL	[El/H]	σ	NL	[El/H]	σ	NL
O I	**−0.05**	−0	1	**−0.10**	–	1	**−0.10**	–	1	**−0.05**	–	1	**−0.10**	–	1	**−0.00**	–	1
Na I	**−0.09**	−0	4	**−0.21**	–	4	**−0.21**	–	4	**−0.13**	–	4	**−0.16**	–	4	**−0.13**	–	4
Mg I	**−0.19**	−0	7	**−0.25**	–	7	**−0.25**	–	7	**−0.24**	–	7	**−0.23**	–	7	**−0.20**	–	7
Al I	0.04	0.01	2	−0.11	0.07	2	−0.02	0.11	2	−0.03	0.02	2	−0.03	0.03	2	0.01	0.10	2
Si I	−0.18	0.09	13	−0.15	0.07	15	−0.05	0.16	17	−0.22	0.14	17	−0.19	0.13	19	−0.15	0.13	20
Ca I	−0.17	0.10	12	−0.17	0.08	12	−0.10	0.19	7	−0.22	0.11	15	−0.13	0.08	12	−0.16	0.08	14
Sc II	−0.16	0.15	8	−0.13	0.13	13	−0.18	0.12	9	−0.07	0.10	8	−0.07	0.06	11	−0.08	0.21	13
Ti I	−0.28	0.15	37	−0.28	0.11	38	−0.19	0.16	24	−0.17	0.10	27	−0.24	0.12	33	−0.27	0.13	31
Ti II	−0.11	0.03	3	−0.05	0.08	4	−0.18	0.12	4	−0.11	0.01	2	0.02	0.04	2	−0.01	0.11	4
V I	−0.26	0.07	20	−0.25	0.11	24	−0.23	0.09	16	−0.22	0.10	16	−0.23	0.14	19	−0.26	0.07	16
Cr I	−0.27	0.15	18	−0.30	0.08	10	−0.26	0.19	13	−0.27	0.13	9	−0.31	0.13	11	−0.24	0.12	9
Fe I	−0.22	0.10	132	−0.22	0.11	157	−0.21	0.17	99	−0.19	0.13	137	−0.22	0.13	121	−0.24	0.12	193
Fe II	−0.28	0.09	5	−0.27	0.10	9	−0.26	0.18	4	−0.25	0.08	6	−0.28	0.11	9	−0.28	0.16	13
Co I	−0.24	0.14	17	−0.26	0.13	21	−0.28	0.17	10	−0.24	0.14	17	−0.27	0.14	18	−0.29	0.14	26
Ni I	−0.25	0.10	52	−0.27	0.12	60	−0.26	0.51	32	−0.26	0.16	41	−0.31	0.11	39	−0.29	0.11	61
Y II	−0.02	0.10	8	−0.11	0.15	9	−0.23	0.14	4	−0.07	0.19	7	−0.11	0.13	14	−0.06	0.12	7
Zr II	−0.07	0.11	2	−0.04	0.15	3	−0.11	0.14	2	−0.15	0.01	2	−0.23	0.00	1	−0.17	0.02	2
Ba II	**0.13**	–	3	**0.25**	–	3	**0.21**	–	3	**0.17**	–	3	**0.05**	–	3	**0.27**	–	3
La II	0.03	0.07	2	0.06	0.01	2	−0.01	0.00	1	0.02	0.00	2	0.04	0.10	2	−0.03	0.06	2
Ce II	0.12	0.18	7	−0.08	0.08	9	0.33	0.16	3	−0.07	0.15	5	−0.01	0.26	8	0.00	0.18	8
Nd II	0.04	0.17	9	0.00	0.14	10	−0.04	0.14	6	0.18	0.21	9	−0.05	0.11	7	−0.08	0.13	10
Eu II	**0.10**	–	1	**0.05**	–	1	**0.25**	–	1	**0.25**	–	1	**0.15**	–	1	**0.15**	–	1

Notes. The abundance values computed with synthetic spectrum marked as bold.

NGC 2477. This cluster has an average reddening $E(B-V)$ = 0.29 (Hartwick, Hesser & McClure 1972), and more recent estimates confirm this early result. Bragaglia et al. (2008) determined a metallicity [Fe/H] = +0.07 ± 0.03 and [Ba/Fe] = 0.46 ± 0.05. [Y/Fe] = 0.21 ± 0.09 was found by Maiorca et al. (2011).

In our case, we obtained [Fe/H] = +0.15, and we detected only a slight excess of [Ba/Fe] = 0.15, while [Y/Fe] = −0.05 and [La/Fe] = 0.08 are close to solar. In particular, the [Ba/Fe] that we calculated is about 0.3 dex lower than Bragaglia et al. (2008).

C14 derived a mean iron content of [Fe/H] = 0.09, or [Fe/H] = 0.04 adopting the same solar iron content adopted here.

NGC 2506. $E(B-V)$ is the range 0.0−0.07 (Marconi et al. 1997). Several estimates of iron abundance are available: [Fe/H] = −0.44 ± 0.06 (Friel et al. 2002), [Fe/H] = −0.20 ± 0.02 (from two stars; Carretta et al. 2004), [Fe/H] = −0.19 ± 0.06 (Reddy et al. 2012), [Fe/H] = −0.24 ± 0.05 (Mikolaitis et al. 2012). Reddy et al. (2012) provided the following estimates for *n*-capture element abundance: [Y/Fe] = 0.04 ± 0.07, [Ba/Fe] = 0.31, [La/Fe] = 0.28 ±

Table 10. Abundance results for NGC 5822.

	1329			1645			1889			2397		
Ion	[El/H]	σ	NL	[El/H]	σ	NL	[El/H]	σ	NL	[El/H]	σ	NL
O I	**0.20**	–	1	**0.15**	–	1	**0.10**	–	1	**0.20**	–	1
Na I	**0.11**	–	4	**0.09**	–	4	**0.07**	–	4	**0.04**	–	4
Mg I	**0.00**	–	7	**−0.03**	–	7	**−0.03**	–	7	**−0.08**	–	7
Al I	−0.03	0.01	2	−0.05	0.08	2	0.03	0.03	2	−0.05	0.08	2
Si I	0.07	0.13	22	0.00	0.11	18	−0.01	0.13	20	0.02	0.16	22
Ca I	0.03	0.08	16	−0.02	0.06	16	0.05	0.09	16	0.04	0.09	17
Sc II	0.07	0.17	13	−0.03	0.11	10	−0.12	0.13	8	0.01	0.14	10
Ti I	−0.07	0.13	64	−0.13	0.08	53	−0.13	0.08	50	−0.09	0.11	55
Ti II	0.05	0.12	5	0.03	0.06	5	0.04	0.14	3	0.06	0.11	4
V I	−0.16	0.09	34	−0.20	0.10	33	−0.18	0.12	33	−0.20	0.10	35
Cr I	−0.09	0.12	37	−0.13	0.09	33	−0.15	0.12	33	−0.13	0.09	35
Cr II	0.11	0.14	2	0.18	0.07	5	0.14	0.17	5	0.23	0.10	4
Fe I	0.04	0.07	211	−0.02	0.09	242	−0.02	0.09	235	0.02	0.09	253
Fe II	0.02	0.05	23	−0.03	0.13	9	0.00	0.06	8	0.04	0.08	8
Co I	−0.02	0.12	26	−0.07	0.13	26	−0.07	0.10	23	−0.07	0.13	26
Ni I	−0.01	0.08	76	−0.05	0.09	76	−0.06	0.09	72	−0.04	0.08	72
Y II	0.22	0.10	9	0.07	0.09	5	0.13	0.10	6	0.22	0.15	6
Zr II	0.13	0.08	4	0.09	0.14	3	−0.02	0.15	3	0.09	0.14	3
Ba II	**0.42**	–	3	**0.38**	–	3	**0.36**	–	3	**0.41**	–	3
La II	0.23	0.06	2	0.15	0.05	2	0.10	0.00	1	0.16	0.03	2
Ce II	0.15	0.06	8	0.09	0.06	7	−0.01	0.11	7	0.08	0.08	7
Nd II	0.16	0.14	13	0.09	0.11	11	−0.01	0.11	10	0.08	0.13	12
Eu II	**0.15**	–	1	**0.10**	–	1	**0.00**	–	1	**0.05**	–	1

Notes. The abundance values computed with synthetic spectrum marked as bold.

Table 11. The mean elemental abundances in OCs.

	Cr 110		Cr 261		NGC 2477		NGC 2506		NGC 5822	
Ion	[El/H]	σ	[El/H]	σ	[El/H]	σ	[El/H]	σ	[El/H]	σ
O I	0.05	–	–	–	−0.13	–	−0.06	–	0.17	–
Na I	−0.02	–	0.13	–	0.12	–	−0.14	–	0.07	–
Mg I	−0.07	–	0.04	–	−0.03	–	−0.22	–	−0.04	–
Al I	0.04	0.04	0.10	0.09	−0.08	0.08	−0.02	0.05	−0.02	0.04
Si I	0.03	0.12	0.05	0.13	0.17	0.16	−0.18	0.12	0.03	0.14
Ca I	−0.02	0.11	−0.03	0.11	0.07	0.14	−0.17	0.09	0.04	0.09
Sc II	−0.03	0.14	0.08	0.12	–	–	−0.10	0.13	0.00	0.15
Ti I	−0.04	0.10	0.04	0.13	−0.01	0.08	−0.25	0.12	−0.09	0.11
Ti II	−0.00	0.11	0.07	0.07	0.11	0.15	−0.05	0.06	0.05	0.12
V I	−0.05	0.10	0.09	0.12	0.07	0.13	−0.24	0.10	−0.18	0.10
Cr I	−0.01	0.09	0.01	0.10	0.04	0.12	−0.28	0.13	−0.12	0.11
Fe I	−0.02	0.11	−0.01	0.11	0.17	0.11	−0.22	0.12	0.01	0.08
Fe II	−0.10	0.09	−0.07	0.09	0.13	0.14	−0.27	0.12	0.02	0.06
Co I	−0.05	0.09	0.03	0.16	0.14	0.11	−0.26	0.14	−0.05	0.12
Ni I	−0.06	0.10	0.04	0.11	0.12	0.10	−0.28	0.12	−0.04	0.08
Y II	0.06	0.12	0.07	0.18	0.11	0.15	−0.08	0.14	0.19	0.11
Zr II	0.03	0.13	0.06	0.13	0.15	0.11	−0.11	0.07	0.07	0.12
Ba II	0.32	–	0.32	–	0.28	–	0.17	–	0.40	–
La II	0.15	0.08	0.14	0.06	0.23	0.03	0.02	0.05	0.18	0.04
Ce II	0.12	0.14	0.06	0.16	0.16	0.16	−0.01	0.17	0.08	0.08
Nd II	0.08	0.11	0.06	0.14	0.07	0.15	0.02	0.15	0.08	0.13
Eu II	0.20	–	0.25	–	0.17	–	0.14	–	0.07	–

0.4, [Ce/Fe] = 0.18, [Nd/Fe] = 0.16 ± 0.06, [Sm/Fe] = 0.22, and [Eu/Fe] = 0.22. On the other hand, Mikolaitis et al. (2012) provided [Ba/Fe] = 0.04 ± 0.10 and [Eu/Fe] = 0.20 ± 0.03.

Our analysis yields a mean value of [Fe/H] = −0.22, an excess of [Ba/Fe] = 0.40, and [Y/Fe] = 0.12, and [La/Fe] = 0.24. Our [Ba/Fe] is about 0.1 dex higher than Reddy et al., and almost 0.4 dex higher than Mikolaitis et al. (2012).

NGC 5822. The value of $E(B-V)$ is in the range 0.10–0.15 (Carrera & Pancino 2011), while metallicity is measured as [Fe/H] = 0.04 (Smiljanic et al. 2009), [Fe/H] = 0.05 (Pace et al. 2010), and [Fe/H] = −0.058 ± 0.027 (Carrera & Pancino 2011). [La/Fe] = 0.31 ± 0.01 was found by Maiorca et al. (2011).

We obtained the mean values of [Fe/H] = 0.01, an excess of [Ba/Fe] = 0.39 and lower excesses for Y and La, with [Y/Fe] =

0.12 and [La/Fe] = 0.13. C14 derived a mean iron content of [Fe/H] = 0.02, or [Fe/H] = −0.03 for the same solar iron content adopted here.

6 RESULTS AND DISCUSSION

The main result from previous works is that [Ba/Fe] is larger than solar for a number of OCs. In particular, the [Ba/Fe] spread tends to increase with decreasing the OCs age, with younger associations showing the largest overabundances (D'Orazi et al. 2009; Yong et al. 2012; Jacobson & Friel 2013, etc). More in general, OCs show a larger spread of Ba enrichment compared to disc stars with similar age (Mishenina et al. 2013a, Mishenina et al. 2013b, 2014). We compared our findings with the results of other authors (Tables 12–14), as well as data obtained in other studies (Table 15). While for a number of OCs, good agreement is obtained, within the observational errors, for other cases a significant departure is observed in the results by different authors. This variation is due to a number of reasons, including e.g. the quality and methods of processing the spectra, atmospheric parameters, the used atomic parameters, especially the oscillator strengths and damping constants, physical approaches LTE or NLTE, model atmospheres, and code abundance computations. This issue was extensively discussed in previous works (e.g. Friel, Jacobson & Pilachowski 2010; Yong, Carney & Friel 2012): the lack of a homogeneous analysis and systematic abundance differences can be much larger than the expected observational errors. For the discussion in this section, we use the data of other authors in their original form, without any correction. Indeed, it is difficult to determine the cause of the difference case by case. On the other hand, we will discuss the larger discrepancies.

Within the uncertainties, the Y enrichment is consistent with disc stars, and consistent with the Sun within 0.2 dex. Therefore, it does not seem that there is any significant anomaly in the Y abundance in OCs (Pancino et al. 2010; Maiorca et al. 2011; Mishenina et al. 2013a).

Table 12. Comparison of our results for star 2129 in Cr 110 with that obtained by Pancino et al. (2010).

Ion	[El/H] (our)	σ	NL	[El/H] (Pan2010)	σ
O I	**0.05**	–	1	−0.02	0.12
Na I	**−0.02**	–	4	−0.01	0.08
Mg I	**−0.07**	–	7	0.06	0.14
Al I	0.10	0.05	2	0.01	0.08
Si I	0.00	0.13	17	0.09	0.02
Ca I	−0.06	0.11	12	0.01	0.04
Sc II	−0.09	0.07	8	−0.02	0.06
Ti I	−0.04	0.08	25	0.05	0.03
Ti II	−0.09	0.14	4	−0.04	0.07
V I	−0.03	0.09	19	0.02	0.05
Cr I	−0.01	0.06	7	0.01	0.06
Fe I	−0.04	0.09	119	0.05	0.01
Fe II	−0.07	0.07	7	−0.04	0.08
Co I	−0.05	0.10	13	−0.03	0.04
Ni I	−0.09	0.07	37	−0.06	0.02
Y II	0.01	0.14	8	−0.12	0.08
Zr II	−0.09	0.18	3	0.00	0.15
Ba II	**0.31**	–	3	0.54	0.04
La II	0.10	0.05	3	0.12	0.03
Ce II	0.09	0.09	3	0.02	0.12
Nd II	0.03	0.11	9	0.29	0.13
Eu II	**0.16**	–	1	–	–

Table 13. Comparison of our results for star 3231 in NGC 2506 with that obtained by Reddy et al. (2012).

Ion	[El/H] (our)	σ	NL	[El/H] (Reddy2012)	σ	NL
O I	**−0.10**	–	1	−0.19	–	1
Na I	**−0.16**	–	4	−0.11	0.08	5
Mg I	**−0.23**	–	7	−0.22	0.07	3
Al I	−0.03	0.03	2	−0.06	0.03	2
Si I	−0.19	0.13	19	−0.22	0.08	7
Ca I	−0.13	0.08	12	−0.16	0.09	9
Sc II	−0.07	0.06	11	−0.16	0.09	5
Ti I	−0.24	0.12	33	−0.26	0.09	9
Ti II	0.02	0.04	2	−0.12	0.06	6
V I	−0.23	0.14	19	−0.20	0.07	8
Cr I	−0.31	0.13	11	−0.27	0.12	9
Fe I	−0.22	0.13	121	−0.25	0.06	38
Fe II	−0.28	0.11	9	−0.22	0.06	8
Co I	−0.27	0.14	18	−0.30	0.14	26
Ni I	−0.31	0.11	39	−0.34	0.11	61
Y II	−0.11	0.13	14	−0.22	0.12	1
Zr II	−0.23	0.00	1	–	–	–
Ba II	**0.05**	–	3	0.06	–	–
La II	0.04	0.10	2	0.06	0.07	1
Ce II	−0.01	0.26	8	–	–	–
Nd II	−0.05	0.11	7	−0.08	0.13	10
Eu II	**0.15**	–	1	0.01	–	–

Table 14. Comparison of our results for stars 2291 and 2311 in Cr 261 with that obtained by de Silva et al. (2007).

	2291		2311	
Ion	log A (our)	log A (DS2007)	log A (our)	log A (DS2007)
Na I	6.44	6.45	6.39	6.65
Mg I	7.61	7.67	7.62	7.89
Si I	7.60	7.66	7.60	7.85
Ca I	6.29	6.29	6.38	6.61
Fe I	7.57	7.51	7.55	7.56
Fe II	7.53	–	7.48	–
Ni I	6.31	6.19	6.37	6.33
Ba II	2.57	2.13	2.53	2.37

The situation is partially different for La. While a number of OCs are consistent with the average of the stars in the disc, a significant fraction shows a [La/Fe] about 0.2–0.3 dex larger than in the Sun. These departures are beyond the present error estimations, but they could be explained within the present systematic uncertainties highlighted comparing the results from different authors (e.g. Yong et al. 2012; Jacobson & Friel 2013, and references therein).

On the other hand, as discussed in Mishenina et al. (2013b) for thin disc stars, the interpretation of the trend of neutron-capture elements with respect to Fe needs to also take into account that Fe is not a fully primary element at high metallicities. In particular, the production of Fe in thermonuclear supernovae (SNIa, Nomoto, Kobayashi & Tominaga 2013, and references therein) is decreasing with increasing initial metallicity of the SNIa progenitor (e.g. Timmes, Brown & Truran 2003; Travaglio, Hillebrandt & Reinecke 2005; Bravo et al. 2010). This theoretical prediction is confirmed by the observation of the [Ni/Fe] increasing trend for supersolar thin disc stars, where the bulk of Ni is instead fully primary (see discussion in Mishenina et al. 2013b). Therefore, with respect to

Table 15. Comparison of the data obtained in the works of various authors.

	[Fe/H]	[Ba/Fe]	[Y/Fe]	[La/Fe]	Ref.
Cr 110	−0.02	0.34	0.08	0.16	this work
	0.03	0.49	0.10	0.03	Pancino et al. (2010)
Cr 261	−0.01	0.33	0.07	0.13	this work
	−0.03	0.30	–	–	Carretta et al. (2005)
	−0.03	0.03	–	–	De Silva et al. (2007)*
	0.13	–	−0.21	–	Maiorca et al. (2011)
	0.13	0.22	–	–	D'Orazi et al. (2009)
NGC 752	0.01	0.19	–	–	D'Orazi et al. (2009)
	−0.02	0.13	0.04	–	Reddy et al. (2012)
	0.08	0.52	−0.03	0.18	Carrera & Pancino (2011)
NGC 2141	−0.09	0.41	–	0.01	Jacobson & Friel (2013)
	−0.18	0.91	–	0.57	Yong, Carney & Teixera de Almeida (2005)
NGC 2477	0.18	0.18	0.12	0.16	this work
	0.07	0.46	–	–	Bragaglia et al. (2008)
	0.07	–	0.21	–	Maiorca et al. (2011)
NGC 2506	−0.22	0.40	0.12	0.24	this work
	−0.19	0.31	0.04	0.28	Reddy et al. (2012)
	−0.24	0.04	–	–	Mikolaitis et al. (2012)*
NGC 2660	0.04	0.47	–	–	D'Orazi et al. (2009)
	0.04	0.61	–	–	Bragaglia et al. (2008)
	0.04	–	0.15	–	Maiorca et al. (2011)
NGC 5822	0.01	0.39	0.12	0.13	this work
	0.05	–	–	0.31	Maiorca et al. (2011)
Be 18	−0.44	0.30	–	0.34	Yong et al. (2012)
	−0.32	0.41	–	0.14	Jacobson & Friel (2013)
Be 20	−0.45	0.14	–	0.30	Yong et al. (2005)
	−0.30	0.09	–	–	D'Orazi et al. (2009)
	−0.30	–	−0.13	–	Maiorca et al. (2011)
Be 21	−0.30	0.58	–	0.56	Yong et al. (2012)
	−0.21	0.50	–	0.14	Jacobson & Friel (2013)
Be 22	−0.44	0.60	–	0.37	Yong et al. (2012)
	−0.24	0.45	–	0.18	Jacobson & Friel (2013)
Be 29	−0.31	0.40	–	–	D'Orazi et al. (2009)
	−0.54	0.30	–	–	Yong et al. (2005)
	−0.31	–	0.35	–	Maiorca et al. (2011)
Be 32	−0.30	0.51	−0.23	−0.14	Carrera & Pancino (2011)
	−0.29	0.24	–	–	D'Orazi et al. (2009)
	−0.29	–	−0.04	–	Maiorca et al. (2011)
	−0.37	0.29	–	0.43	Yong et al. (2012)
	−0.27	0.22	–	−0.08	Jacobson & Friel (2013)
	−0.29	0.29	–	–	Bragaglia et al. (2008)
Hyades	0.11	0.36	−0.09	−0.08	Carrera & Pancino (2011)
	0.13	0.30	–	–	D'Orazi et al. (2009)
	0.13	–	0.12	–	Maiorca et al. (2011)
Praesepe	0.16	0.33	−0.11	−0.05	Carrera & Pancino (2011)
	0.27	0.22	–	–	D'Orazi et al. (2009)
	0.27	–	-0.01	–	Maiorca et al. (2011)
M 67	0.03	–	0.01	0.06	Maiorca et al. (2011)
	0.05	0.25	−0.05	0.05	Pancino et al. (2010)
	0.02	0.04	–	–	D'Orazi et al. (2009)
	0.05	0.10	–	−0.15	Jacobson & Friel (2013)
	−0.01	−0.02	–	0.11	Yong et al. (2005)
	−0.08	−0.16	0.03	0.00	Reddy, Giridhar & Lambert (2013)
PWM4	−0.34	0.36	–	0.22	Yong et al. (2012)
	−0.18	0.34	–	0.05	Jacobson & Friel (2013)

Notes: * These data are not all included in the figures. See the text.

the Sun, a scatter of neutron-capture elements compared to Fe may be expected in the disc and in OCs, depending on the Fe enrichment history. The quantification of this intrinsic scatter due to the Fe production from SNIa needs to be estimated by galactical chemical evolution simulations, that take into account present uncertainties affecting theoretical SNIa yields.

We cannot exclude that our sample is affected by observational issues, especially for La. In Table 4, we have shown that the expected uncertainty for the [La/Fe] is about 0.1 dex. On the other hand, there are much larger differences for La between different works (e.g. Jacobson & Friel 2013). Among others, there is the example of NGC 2141. Be 31 and NGC 2141 show a [La/Fe] that is much

larger than other observed OCs: [La/Fe] = 0.91 and 0.57 (Yong et al. 2005). The same OCs show extremely high [Ba/Fe] = 0.64 (Be 31) and 0.91 (NGC 2141), and for [Eu/Fe] = 0.56 (Be 31) and 0.17 (NGC 2141). At the end of this section, we will discuss again these two special cases.

For the element Eu, considered as a typical *r*-process element, we found abundances consistent with the Solar system and with the average of the disc.

In order to derive additional observational constrains for stellar simulations and the chemical enrichment history of OCs, we combined here the results of our analysis with data collected from the literature, and build up the largest sample to date of high-resolution abundances of neutron-capture elements.

In Fig. 3, we show the trend of [Ba/Fe], [La/Fe] and [Y/Fe] versus [Fe/H] for all the OCs available, and we include also Melotte 66 (Carraro et al. 2014), and Trumpler 5 (Monaco et al. 2014). In the figures, the abundance values obtained for the same cluster and having the difference between these values more than the errors given in Table 4 are connected by a line.

In Fig. 4, the [Ba/Fe], [La/Fe], and [Y/Fe] are also shown as a function of the cluster ages. The ages were calculated consistently, according to Carraro & Chiosi (1994). In the figures, we include abundances obtained earlier (Mishenina et al. 2013a, 2014) with measurements from other authors, for a number of OCs (Yong et al. 2005; Bragaglia et al. 2008; D'Orazi et al. 2009, 2012; Pancino et al. 2010; Carrera & Pancino 2011; Maiorca et al. 2011; Reddy et al. 2012, 2013; Jacobson & Friel 2013) and the data for the thin disc stars were taken from the study by Mishenina et al. (2013b).

Within the errors, we cannot observe any specific trend with age for Y and La. This result is consistent with previous works, e.g. Jacobson & Friel (2013). Yong et al. (2012) discussed about a possible increasing trend of La with the age of OCs, but they also stressed about the large uncertainties and their potential impact on those results. On the other hand, we confirm the increasing average trend of [Ba/Fe] for younger OCs, in agreement with previous works.

OCs measured by two independent groups with differences larger than the error reported in Table 4, are connected with a line. In the case when the values obtained by different authors lie within the errors, in the figures we only report the values obtained in this work, Mishenina et al. (2013a), D'Orazi et al. (2009), D'Orazi et al. (2012), and Maiorca et al. (2011). A remarkable case is NGC2141, where differences between Yong et al. (2005) and Jacobson & Friel (2013) are about 0.5 and 0.6 dex for [Ba/Fe] and [La/Fe], respectively. These large differences are due in part from an average done by Jacobson & Friel (2013) between two stars, 1007 and 1348, with 1007 showing a moderate Ba enrichment and a negative [La/Fe]. On the other hand, considering only the star 1348 in common between the two authors, Yong et al. (2005) reported [Ba/Fe] and [La/Fe] that are 0.4 and 0.44 dex larger than Jacobson & Friel (2013). While the differences affecting the Ba determination are already quite large but they can be understood (according to their table 3, Jacobson & Friel 2013 used the Ba lines 5853, 6141, and 6496 ÅÅ, with significant differences in the resulting Ba abundances, while the abundance obtained from the line 5853 Å in common with Yong et al. 2005 shows a better agreement), we find more difficult to explain this discrepancy for La.

Despite these large differences, the conclusions concerning the nature of the neutron-capture nucleosynthesis signature in NGC 2141 will not change considering Yong et al. (2005) or Jacobson & Friel (2013) observations.

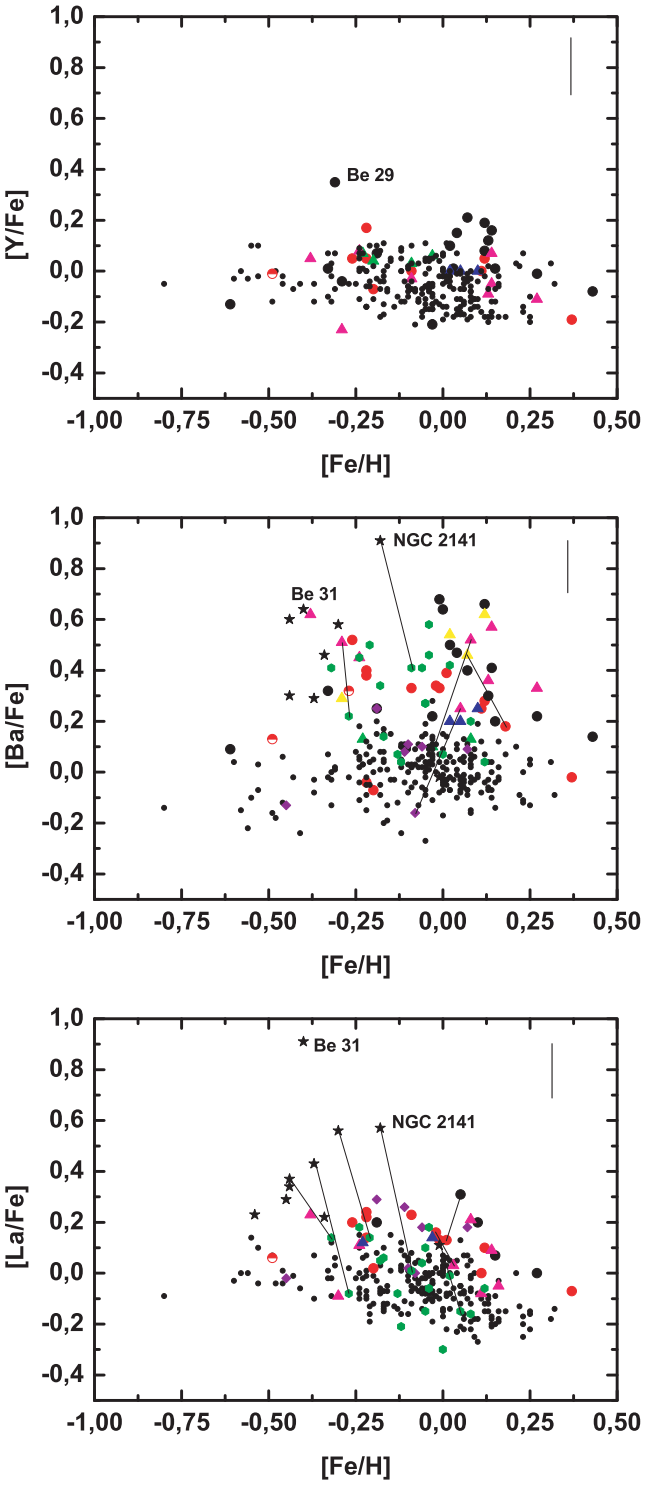

Figure 3. The trend of [Y/Fe] (upper panel), [Ba/Fe] (central panel), and [La/Fe] (lower panel) versus [Fe/H]. Symbols are as follows: Y and La abundances by Maiorca et al. (2011) and Ba abundances by D'Orazi et al. (2009): black circles; Pancino et al. (2010) and Carrera & Pancino (2011): magenta triangles; D'Orazi et al. (2012): blue triangles; Reddy et al. (2012): green triangles. Ba abundances by Bragaglia et al. (2008): yellow triangles; Yong et al. (2005, 2012): asterisks; Reddy et al. (2013): violet rhombuses; Jacobson & Friel (2013): olive diamonds; Carraro et al. (2014) and Monaco et al. (2014): semifull red cirles; Mishenina et al. (2013b): the thin disc (marked as black dots); finally, our determinations (Mishenina et al. 2013a; Mishenina et al. 2014) and this study: red circles.

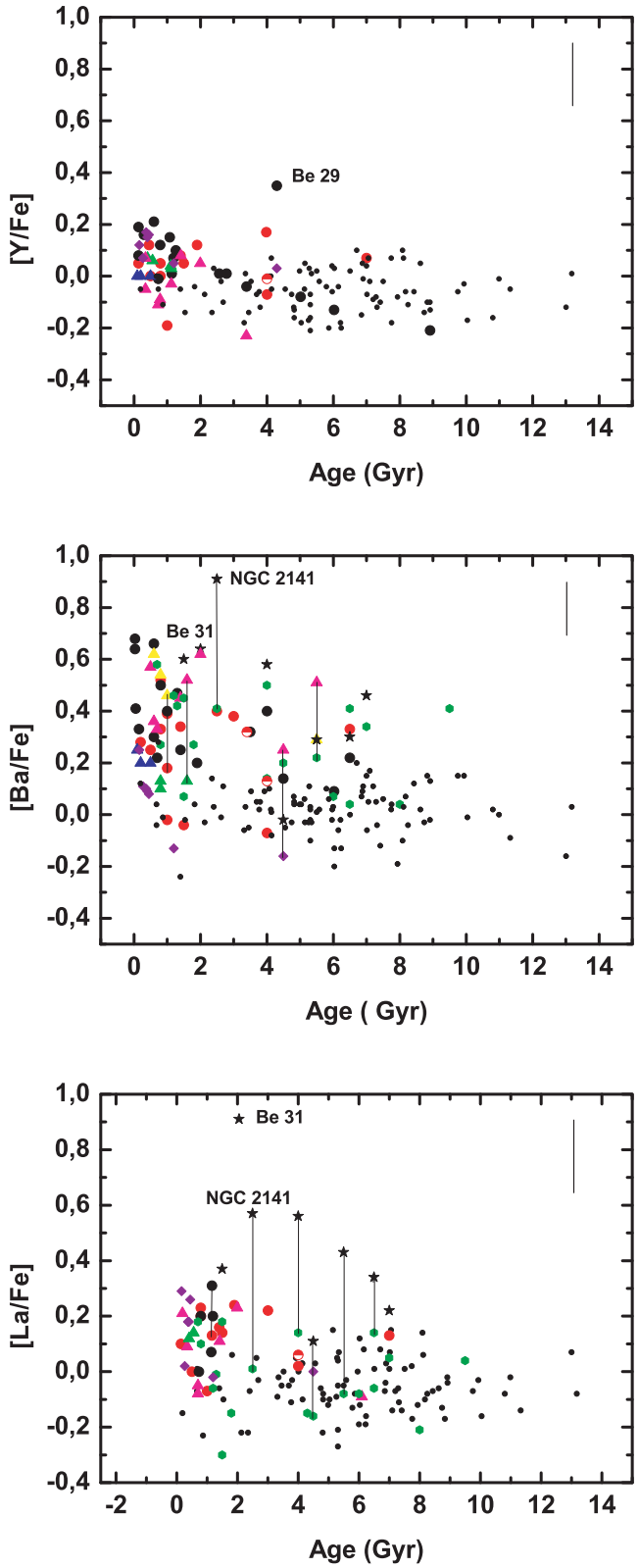

Figure 4. The trend of [Y/Fe], [La/Fe], and [Ba/Fe] are reported compared to the age. The age values were obtained in the uniform scale as in Carraro & Chiosi (1994). Symbols for different observations are reported as in Fig. 3.

As for [Ba/Fe], three other OCs showing a significant departure are: NGC 752 – [Ba/Fe] = 0.13 (Reddy et al. 2012) and [Ba/Fe] = 0.52 (Carrera & Pancino 2011); Be 32 – [Ba/Fe] = 0.22 (Jacobson & Friel 2013) and [Ba/Fe] = 0.51 (Carrera & Pancino 2011); NGC 2477 – [Ba/Fe] = 0.18 (this work) and [Ba/Fe] = 0.48 (Bragaglia et al. 2008). Concerning La, large departures are present between Yong et al. (2012) and Jacobson & Friel (2013) for most of the common OCs, with the first authors obtaining a larger La abundance.

In Fig. 4, the increasing spread of Ba enrichment towards younger OCs and on average the much stronger enrichment of Ba compared to La is confirmed within this larger sample of OCs. This is difficult to explain in term of neutron-capture nucleosynthesis. The production of Ba and La by neutron-capture processes is similar. Ba and La are mostly made by their stable isotopes ^{138}Ba and ^{139}La, located at the neutron shell closure $N = 82$. They are commonly indicated as *s*-process elements, since most of their abundance in the Solar system is explained by the *s*-process in asymptotic giant branch (AGB) stars. In particular, according to galactical chemical evolution simulations, about 85.2 and 75.5 per cent of solar Ba and La are made by the *s*-process (Bisterzo et al. 2014). Applying the residual method where the solar abundance of heavy elements beyond Fe is given by the contribution of the *s*-process and the *r*-process (e.g. Arlandini et al. 1999), the fraction of Ba and La made by the *r*-process are 14.8 and 24.5 per cent, respectively. Therefore, the fact that Ba and La seem to have a different behaviour is puzzling. Maiorca et al. (2012) proposed that the heavy elements enrichment observed in young OCs is a signature of a larger *s*-process enrichment from low-mass AGB stars compared to the Solar system, and Trippella et al. (2014) explored the impact of magnetic buoyancy as a mechanism to trigger more efficient *s*-process production, allowing more extended radiative ^{13}C-pockets to form. Nevertheless, an additional *s*-process contribution should not cause anomalies for the Ba/La ratio compared to established *s*-process calculations. A larger enrichment of Ba compared to La it is difficult to reconcile with *s*-process and *r*-process nucleosynthesis, or with a different combination of these two components compared to the Solar system. To better explain this point, in Fig. 5 we show the [Ba/La] compared to [La/Eu] for the OCs and the disc stars. The pure *s*-process and *r*-process ratios are shown for comparison from Travaglio et al. (2004) and Bisterzo et al. (2014).

Within the scenario where the heavy elements are made by a combination of these two processes, the observations should fall inside the box, drawn by the assumptions of pure *s*-process or *r*-process contributions. This is not the case for a sample of disc stars, and in particular for the most Ba-rich OCs. From this figure, it is clear that an additional *s*-process component cannot be the explanation of these anomalous abundances, since in this scenario the observations would still plot between the Solar system and the pure *s*-process lines. In Fig. 5, we also show the [Ba/La] with respect to the age of the OCs. While there could be a mild increase of the [Ba/La] ratio towards younger OCs, within the present uncertainties we cannot derive any clear conclusion.

Three possible solutions to this puzzle are the following: (1) the measured Ba abundance for Ba-rich OCs (and part of the disc stars) is overestimated; (2) the measured La abundance is underestimated; (3) an additional neutron-capture component different from the *s*-process and the *r*-process is contributing to the economy of heavy elements, producing more efficiently Ba than La and Eu.

Concerning the first option, we have discussed the possible sources of uncertainty affecting the estimation of the Ba abundance in Section 5. Here, we just remind that we have considered

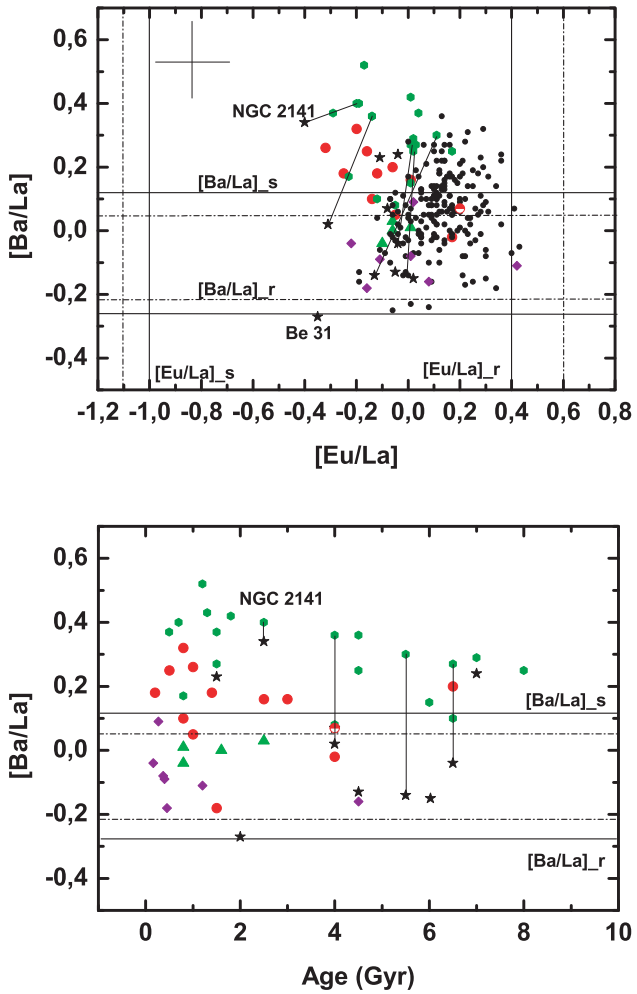

Figure 5. Upper panel: the [Ba/La] ratio for a sample of OCs and disc stars is plotted with respect to the [Eu/La]. The pure *s*-process and *r*-process ratios are indicated in the figure, according to Bisterzo et al. (2014, dotted lines) and Travaglio et al. (2004, solid lines). Bottom panel: the [Ba/La] ratio versus age for a sample of OCs.

NLTE effect for our analysis. Overall, we estimated that the uncertainty for Ba should not exceed 0.2 dex (Table 4). On the other hand, for the [Ba/Fe] ratio in the literature we found discrepancies with our measurements in the order of 0.3 dex, and in one case of 0.4 dex (see also the discussion in Jacobson & Friel 2013, and references therein). While we cannot discard this first option, at the moment we would consider quite low the probability that this is the solution of the Ba puzzle. Indeed, among the all considered uncertainties, the NLTE effect is the only one that could explain a systematic overproduction for Ba, while other uncertainties may also yield its underestimation from a given measure. In the measurements reported in this work, we keep into account the NLTE effect. In Section 4, we also discussed the possible issues reported by D'Orazi et al. (2012).

Concerning the second option, the uncertainty affecting the estimation of the La abundance is lower than Ba, in the order of 0.1 dex (Table 4). The La lines adopted for Mishenina et al. (2014) and this work are 6320.41, 6390.48 ÅÅ. There are not blending from other lines. The La abundance was found taking into account the HFS. The structure of electronic levels of La is similar to the structure of the ones of Eu and as Mashonkina (2000) has shown the NLTE corrections are very small for atoms of europium. Therefore, we believe that the NLTE effects in lanthanum abundance are also insignificant.

On the other hand, according to Jacobson & Friel (2013), the use of the EW's leads to reduce the La values by 0.07 dex, with an error of ±0.15 dex. This last option would partly reduce the [Ba/La] ratio, but it cannot explain the highest values shown in Fig. 5. We would consider this last possibility alone unlikely to solve the Ba puzzle, but we need to keep in mind the large differences obtained for the La abundance between different authors mentioned earlier, beyond the observational error.

If the first option is correct, the present observations in OCs would be easier to reconcile with GCE calculations using baseline AGB models and more in general with the prediction from the residual method. If the second option is correct, and the Eu observations are confirmed compared to Fe, in order to explain the heavy element abundances in OCs a stronger *s*-process contribution may be needed, compared to the Solar system. As we mentioned before, a solution has been proposed within the present uncertainties on the physics mechanisms responsible for the formation of the ^{13}C-pocket in AGB stars. We could also argue that in order to reconcile the large observed [Ba/La] with theoretical *s*-process predictions, both the first and the second option are correct. In summary, at the moment it is not clear how to explain a [Ba/La] up to 0.35 dex systematically higher than the pure *s*-process theoretical value, and major observational issues would be required.

In case observations of Ba and La are correct, then this may be the first evidence of an additional neutron-capture process contributing to the GCE of heavy elements. From Fig. 5, nor the *s*-process or the *r*-process can explain a [Ba/La] larger than ∼0.15 dex. In this case, the scenario that we propose is the additional contribution from the intermediate neutron-capture process, or *i*-process. First introduced more than 30 yr ago by Cowan & Rose (1977), the *i*-process is characterized by neutron densities of the order of 10^{15} neutrons cm^{-3}. As discussed by Cowan & Rose (1977), the *i*-process is triggered by the mixing or ingestion of H in He-burning stellar layers: protons are captured by the abundant He-burning product ^{12}C forming ^{13}C via the channel ^{12}C(p,γ)^{13}N(β+)^{13}C. ^{13}C is the main source of neutrons via the (α,*n*) reaction rate.

The first observational evidence of *i*-process activation in stars is in the post-AGB Sakurai's object, explaining the anomalous heavy element abundances (Herwig et al. 2011) and the fast change of abundance observed in a short time-scale (Asplund et al. 1999). Additional signature of the *i*-process activation in post-AGB stars is found in pre-solar grains (Jadhav et al. 2013).

Recently, Bertolli et al. (2013) proposed the *i*-process as the source of the anomalous heavy-element signature observed in a sub-sample of carbon-enhanced metal-poor stars, usually explained as a mixture of *s*-process and *r*-process contribution (CEMP-rs stars, e.g. Masseron et al. 2010; Lugaro et al. 2012; Bisterzo et al. 2014). In particular, some of these stars seem to show a [Ba/La] ratio larger than what the *s*-process, the *r*-process or a combination of them can explain.

The *i*-process can potentially explain this larger ratio, where the bulk of Ba is radiogenic, made by the decay of ^{135}I, but major nuclear uncertainties still affect theoretical simulations (Bertolli et al. 2013).

Another major problem is that multidimensional hydrodynamics simulations are needed in order to produce consistent results for the H ingestion in He-burning layers (e.g. Herwig et al. 2007; Mocak, Siess & Muller 2011; Stancliffe et al. 2011; Woodward, Herwig & Lin 2013; Herwig et al. 2014). Baseline hydrostatic stellar models can provide only qualitative information at best about these events,

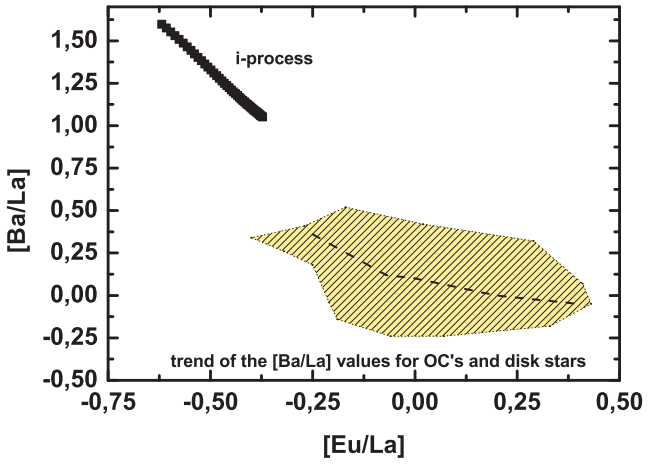

Figure 6. The [Ba/La] trend with respect to the [Eu/La] is shown for the *i*-process trajectory (Bertolli et al. 2013), and for the average of the OCs in the sample considered in this work. The schematic observational distribution for OCs and disc stars is shown. Concerning the *i*-process trajectory, the earlier production of Ba compared to La is given by the radiogenic contribution from ^{135}I to ^{135}Ba. With the increasing of the total amount of neutrons, also La starts to be made and the [Ba/La] tends to decrease.

and without guidance from hydrodynamics simulations fail to reproduce the observations (Herwig et al. 2011).

In Fig. 6, we show the theoretical *i*-process predictions from a simple trajectory reproducing the *i*-process neutron density conditions. This is the same trajectory given by Bertolli et al. (2013), but adopting initial abundances beyond Si compatible with galactic disc metallicity. In particular, the initial ^{56}Fe mass fraction is 5.3×10^{-4}, about half of the ^{56}Fe amount in the Solar system.

In the figure, the trajectory behaviour is shown when [Ba/Y] is larger than 0.7 dex (consistent with observations of Ba-rich OCs), and for Ba five times larger than Pb. The trajectory shows [Ba/La] high values, decreasing with the increasing of the amount of neutrons available. For comparison, we also report the average trend observed for all the OCs, and the observed range covered by OCs and disc stars considered here (see Fig. 5). From Fig. 6, we can argue that a combination of the *i*-process, the *s*-process, and the *r*-process provide a scenario capable to explain the observed large [Ba/La], mainly contributing to Ba compared to Y, La, and Eu.

At the moment, it is difficult to constrain what is(are) the host(s) of the *i*-process. If this scenario is correct, the *i*-process occurrence cannot be limited to H-deficient post-AGB stars (Herwig et al. 2011), or to low-metallicity stellar hosts (Bertolli et al. 2013). For instance, in Pignatari et al. (in preparation), we found proof of late H ingestion in massive stars just before the core-collapse supernovae explosion. The fact that these H-ingestion events in massive stars are also associated with *i*-process production is not clear, and need more investigation.

In Fig. 5, we show that also a relevant fraction of the disc stars show a [Ba/La] larger than the *s*-process limit. In this case, the departure is lower compared to the most Ba-rich OCs, and on average at larger [Eu/La]. As also shown from previous works for OCs and for disc stars (e.g. Bensby et al. 2005; D'Orazi et al. 2009; Jacobson & Friel 2013), the average Ba enrichment seems to increase for objects younger than the Sun. This could suggest that in these last Gyrs, the *i*-process contribution is becoming more relevant than what it was for our Sun, compared to the established *s*-process and *r*-process contribution. On the other hand, as we mentioned earlier, we cannot claim any trend of the [Ba/La] with respect to the age of the OCs (Fig. 5).

Taking into account the previous discussion about observation uncertainties, it is not possible to derive any strong conclusion, claiming that also disc stars are hiding an *i*-process contribution. On the other hand, in case OCs are carrier of an *i*-process component, it would be reasonable to assume that the same is happening for disc stars.

In Fig. 7, we show the [Ba/Fe], [La/Fe], and [Ba/La] distribution for OCs compared to the thin disc stars by Mishenina et al. (2013b). Concerning the [La/Fe] distribution, OCs show a peak shifted by 0.1–0.2 dex compared to thin disc stars. While this difference is not negligible, it is still within the present observational uncertainties.

On the other hand, the [Ba/Fe] in OCs is clearly shifted towards larger values, and the distribution looks more scattered than for disc stars. Note that the present observed scatter is real, represented in our sample of OCs (Mishenina et al. 2013a, and this work), and not a product of observational systematics uncertainties. But concerning the analysis including all the OCs, in agreement with previous works we confirm that the observational uncertainties and the lack of homogeneous abundance analysis is an issue that needs to solved in the future in order to derive definitive conclusions. Finally, the larger [Ba/Fe] spread in OCs compared to disc stars is conserved in the [Ba/La] ratio. The disc stars show a distribution peak 0.1 dex larger than solar, consistent within the uncertainties. For OCs, the peak is much broader, and shifted to larger values. The reason of these differences in the heavy element enrichment between OCs and disc stars has to be analysed with chemical evolution simulations, and it is not the goal of this paper. According to Fig. 5, a possible scenario to explain the observed increase of [Ba/La] with the decreasing of [Eu/La] could be that OCs have overall a smaller contribution from the *r*-process compared to disc stars, highlighting contribution from *s*-process and *i*-process components.

In Figs 3 and 4, we highlighted the OCs Be 31 and NGC 2141 by Yong et al. (2005), showing a [La/Fe] much larger than other OCs (see also Fig. 7). Be 31 is one of the most metal-poor OCs presently known, despite it is not one of the oldest (about 2 Gyr, Carraro & Chiosi 1994). It shows a much larger *s*-process enrichment of *s*-process elements Ba and La compared to the *r*-process element Eu. Yong et al. (2005) explained this as an effect of a significant contribution from AGB stars *s*-process-rich material. The position of Be 31 in Fig. 5 seems to confirm this scenario. The [Eu/La] is consistent with a larger *s*-process contribution compared to the Sun, while the [Ba/La] can be explained by an enrichment history given by the *s*-process and the *r*-process contributions. Within this scenario, due to the relative low metallicity, we would expect that Be 31 has also a larger Pb enrichment compared to the Sun. Therefore, the measurement of Pb would be extremely useful to confirm this scenario. Unfortunately, at the moment there are no available measurements for Pb abundances in OCs. NGC 2141 has an age similar to Be 31, but has a metallicity much closer to the Sun. It may be the most Ba-rich OC within the sample considered in this work but we have shown that large discrepancies are obtained considering different works (e.g. Fig. 4 and Table 15). Within the large uncertainties affecting [Ba/Fe] and [La/Fe], the [Ba/La] is larger than the *s*-process ratio, consistently with the anomalous signature discussed in this work. Assuming that there are no other observational issues for Ba, NGC 2141 is another candidate where the *i*-process contribution can be identified.

7 CONCLUSIONS AND FINAL REMARKS

In this work, we presented and discussed new abundance measurements for five OCs: Cr 110, Cr 261, NGC 2477, NGC 2506, and NGC 5822. We analysed these new results for neutron-capture

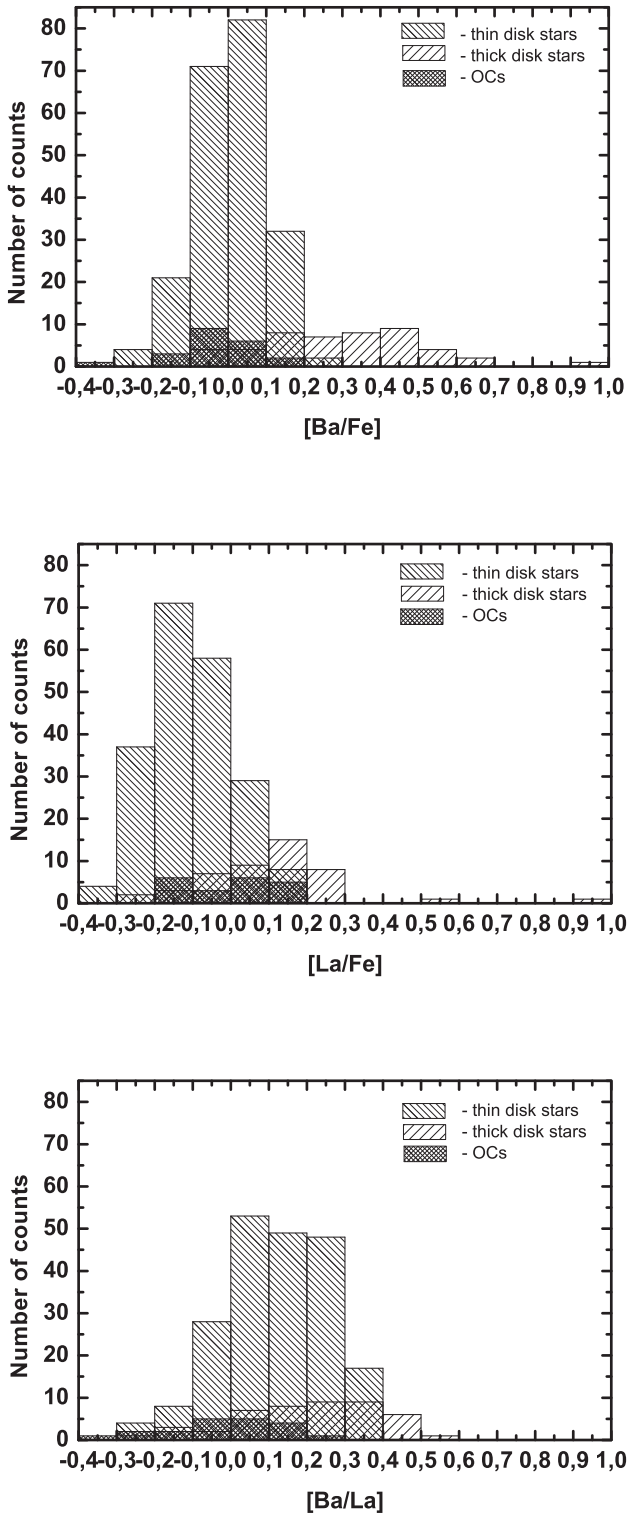

Figure 7. The distribution of the [Ba/Fe], [La/Fe], and [Ba/La] ratio for OCs is shown compared to the thin disc stars and thick disc stars in Mishenina et al. (2013b).

elements complementing them with literature data. Literature data show significant author-to-author differences, that we discussed. Beside these differences, we found confirmation of the larger scatter of the Ba abundance in OCs compared to disc stars. We also confirm that the average Ba abundance is increasing for younger OCs, while there is not clear trend with the metallicity [Fe/H]. To a lower extent, the [La/Fe] ratio seems to show a similar behaviour as Ba.

With the exception of few OCs, the [La/Fe] is found to be consistent with the average disc enrichment. A possible source of uncertainty is, however, the impact of the metallicity dependence of the Fe production from SNIa. This needs future investigations because of its implications for the ratio between neutron-capture elements and Fe in thin-disc stars and OCs. Finally, the [Y/Fe] ratio in OCs is consistent with disc stars and the Sun within the uncertainties.

Besides the overall enrichment of neutron-capture elements compared to Fe, we showed that the resulting [Ba/La] ratio is not consistent with the established scenario for the production of heavy elements, with a combined contribution from the *s*-process and *r*-process only.

The OCs (and to less extent disc stars) show an increasing [Ba/La] ratio for a decreasing [Eu/La], reaching values for [Ba/La] up to 0.4–0.5 dex, much larger than what expected from *s*-process or the *r*-process.

We considered three main options to explain this occurrence.

The first two options are related to possible observational issues with Ba and La. In particular, we discuss possible uncertainties affecting the measurement of the Ba abundance. We argue that the uncertainty in the Ba abundance alone cannot explain the enrichment observed for such a large number of OCs. On the other hand, it might be possible that the La abundance be underestimated, which could help to reconcile the OCs observations within the baseline scenario of an *s*-process and *r*-process contribution. Therefore, the reduction of present observational uncertainties and of the amount of inhomogeneity of the observed data could still solve this puzzle.

In case instead the observations are correct, we considered and discussed a third option: that OCs are showing the additional contribution from the *i*-process. This may be the first evidence that the *i*-process had a relevant contribution to the galactic chemical evolution of the Galaxy, together with the *s*-process and the *r*-process. One of the peculiar signatures of the *i*-process is to predict a [Ba/La] ratio much larger than the *s*-process or the *r*-process, within the observed spread of [Eu/La]. The capability to disentangle the production of Ba and La is a unique feature, caused by neutron densities intermediate between the *s*-process and the *r*-process. We show that the additional contribution from the *i*-process is consistent with the present observations in OCs.

This scenario needs to be corroborated by considering more neutron-capture elements. Despite the fact that the *i*-process was defined more than 30 yr ago, only in the last 5 yr, we are starting to collect observational evidences of its existence in different types of stars at different metallicities, and in pre-solar grains. Furthermore, robust predictions of *i*-process stellar yields cannot be provided by baseline one-dimensional hydrostatic models. The *i*-process is associated with H ingestion in hot He-burning environments, requiring the guidance of multidimensional hydrodynamics simulations. These are challenging and computationally expensive but feasible, as proven from a number of simulations that are becoming available. The impact of present nuclear uncertainties on the *i*-process nucleosynthesis should also be fully explored, if relevant for the observed elemental ratios. We refer to Bertolli et al. (2013) for the nuclear uncertainties affecting the [Ba/La] ratio.

In conclusion, this work provided an important step forward for our understanding of the nucleosynthesis of neutron-capture elements in the Galaxy. More observations are needed for more neutron-capture elements in OCs. On the other hand, when discrepancies larger than about 0.2 dex exist between different

works for the same objects, a new independent analysis would be recommended. It is obvious that the inhomogeneity of the data we gathered from the literature is playing a major obstacle towards a solid understanding of these abundance ratio patterns. Unfortunately, this is the actual situation, and we will need to wait for more extended and homogeneous data set to become available, such as *Gaia*–ESO (Gilmore et al. 2012). Similar conclusions have been derived from other previous works analysing the abundances for an extended sample of OCs. This consensus is an important step to draw the priorities for next observational campaigns.

On the theoretical side, the calculation of robust *i*-process yields for different types of stars are not available at the moment. This will require extensive hydrodynamics simulations for different stellar environments in the coming years, as a guidance for complete sets of one-dimensional hydrostatic stellar models.

ACKNOWLEDGEMENTS

We thank the anonymous referee for a detailed and thoughtful review of our manuscript. TM,SK, and MP thank for the support from the Swiss National Science Foundation, project SCOPES No. IZ73Z0152485. MP and FH acknowledge significant support to NuGrid from NSF grants PHY 02-16783 and PHY 09-22648 (Joint Institute for Nuclear Astrophysics, JINA) and EU MIRG-CT-2006-046520. MP acknowledges an Ambizione grant of the SNSF and support from SNF (Switzerland). FH acknowledges NSERC Discovery Grant funding.

REFERENCES

Arcones A., Montes F., 2011, ApJ, 731, 5
Arlandini C., Käappeler F., Wisshak K., Gallino R., Lugaro M., Busso M., Straniero O., 1999, ApJ, 525, 886
Asplund M., Lambert D. L., Kipper T., Pollacco D., Shetrone M. D., 1999, A&A, 343, 507
Asplund M., Grevesse N., Sauval A. J., Scott P., 2009, ARA&A, 47, 481
Bensby T., Feltzing S., Lundström I., Ilyin I., 2005, A&A, 433, 185
Bensby T. et al., 2009, A&A, 499, 737
Bertolli M. G., Herwig F., Pignatari M., Kawano T., 2013, preprint (arXiv:1310.4578)
Bisterzo S., Travaglio C., Gallino R., Wiescher M., Käppeler F., 2014, ApJ, 787, 10
Bragaglia A., Tosi M., 2003, MNRAS, 343, 306
Bragaglia A., Sestito P., Villanova S., Carretta E., Randich S., Tosi M., 2008, A&A, 480, 79
Bravo E., Dominguez I., Badenes C., Piersanti L., Straniero O., 2010, ApJ, 711, 66
Caffau E. et al., 2014, A&A, 568, A29 (C14)
Cameron A. G. W., 1982, Ap&SS, 82, 123
Carlsson M., 1986, Uppsala Obs. Rep., 33
Carraro G., Chiosi C., 1994, A&A, 287, 761
Carraro G., Anthony-Twarog B., Costa E., Jones B. J., Twarog B., 2011, AJ, 142, 127
Carraro G., de Silva G., Monaco L., Milone A., Mateluna R., 2014, A&A, 566, 39
Carrera R., Pancino E., 2011, A&A, 535, 30
Carrera R., Gallart C., Pancino E., Zinn R., 2007, AJ, 134, 1298
Carretta E., Bragaglia A., Gratton R. G., Tosi M., 2004, A&A, 422, 951
Carretta E., Bragaglia A., Gratton R. G., Tosi M., 2005, A&A, 441, 131
Castelli F., Kurucz R. L., 2004, preprint (astro-ph/0405087)
Coelho P., Barbuy B., Meléndez J., Schiavon R. P., Castilho B. V., 2005, A&A, 443, 735
Cowan J. J., Rose W. K., 1977, ApJ, 212, 149
D'Orazi V., Magrini L., Randich S., Galli D., Busso M., Sestito P., 2009, ApJ, 693, 31
D'Orazi V., Biazzo K., Desidera S., Covino E., Andrievsky S. M., Gratton R. G., 2012, MNRAS, 423, 2789
De Silva G. M., Freeman K. C., Asplund M., Bland-Hawthorn J., Bessel M. S., Collet R., 2007, AJ, 133, 1161
Farouqi K., Kratz K.-L., Mashonkina L. I., Pfeiffer B., Cowan J. J., Thielemann F.-K., Truran J. W., 2009, ApJ, 694, 49
Friel E. D., Janes K. A., Tavarez M., Scott J., Katsanis R., Lotz J., Hong L., Miller Nathan., 2002, AJ, 124, 2693
Friel E. D., Jacobson H. R., Barrett E., Fullton L., Balachandran S. C., Pilachowski C. A., 2003, AJ, 126, 2372
Friel E. D., Jacobson H. R., Pilachowski C. A., 2010, AJ, 139, 1942
Frischknecht U., Hirschi R., Thielemann F.-K., 2012, A&A, 538, 2
Fröhlich C., Martinez-Pinedo G., Liebendorfer M., Thielemann F.-K., Bravo E., Hix W. R., Langanke K., Zinner N. T., 2006, Phys. Rev. Lett., 96, 142502
Galazutdinov G. A., 1992, Preprint SAO RAS, 92, 2
Gilmore G. et al., 2012, The Messenger, 147, 25
Gilmore G., Norris J. E., Monaco L., Yong D., Wyse R. F. G., Geisler D., 2013, ApJ, 763, 61
Gozzoli E., Tosi M., Marconi G., Bragaglia A., 1996, MNRAS, 283, 66
Hansen C. J. et al., 2012, A&A, 545, 28
Hartwick F. D. A., Hesser J. E., McClure R. D., 1972, ApJ, 174, 557
Herwig F., Freytag B., Fuchs T., Hansen J. P., Hueckstaedt R. M., Porter D. H., Timmes F. X., Woodward P. R., 2007, in Kerschbaum F., Charbonnel C., Wing R. F., eds, ASP Conf. Ser. Vol. 378, Why Galaxies Care About AGB Stars: Their Importance as Actors and Probes. Astron. Soc. Pac., San Francisco, p. 43
Herwig F., Pignatari M., Woodward P. R., Porter D. H., Rockefeller G., Fryer C. L., Bennett M., Hirschi R., 2011, ApJ, 727, 89
Herwig F., Woodward P. R., Lin P.-H., Knox M., Fryer C., 2014, ApJ, 792, L3
Hoffman R. D., Woosley S. E., Fuller G. M., Meyer B. S., 1996, ApJ, 460, 478
Jacobson H. R., Friel E. D., 2013, AJ, 145, 107
Jadhav M., Pignatari M., Herwig F., Zinner E., Gallino R., Huss G. R., 2013, ApJ, 777, 27
Janes K. A., Phelps R. J., 1994, AJ, 108, 1773
Käppeler F., Gallino R., Bisterzo S., Aoki W., 2011, Rev. Mod. Phys., 83, 157
Kassis M., Janes K. A., Friel E. D., Phelps R. L., 1997, AJ, 113, 1723
Keeping E. S., 1962, Introduction to Statistical Inference. van Nostrand, Princeton, NJ
Korotin S. A., Mishenina T. V., 1999, Astron. Rep., 43, 533
Korotin S., Mishenina T., Gorbaneva T., Soubiran C., 2011, MNRAS, 415, 2093
Kovtyukh V. V., Soubiran C., Bienaymé O., Mishenina T. V., Belik S. I., 2006, MNRAS, 371, 879
Kupka F., Piskunov N. E., Ryabchikova T. A., Stempels H. C., Weiss W. W., 1999, A&AS, 138, 119
Kurucz R. L., Furenlid I., Brault J., Testerman L., 1984, National Solar Observatory Atlas. National Solar Observatory, New Mexico
Lugaro M., Karakas A., Stancliffe R., Rijs C., 2012, ApJ, 747, 2
Maiorca E., Randich S., Busso M., Magrini L., Palmerini S. E., 2011, ApJ, 736, 120
Maiorca E., Magrini L., Busso M., Randich S., Palmerini S., Trippella O., 2012, ApJ, 747, 53
Marconi G., Hamilton D., Tosi M., Bragaglia A., 1997, MNRAS, 291, 763
Mashonkina L. I., 2000, Astron. Rep., 44, 558
Masseron T., Johnson J. A., Plez B., van Eck S., Primas F., Goriely S., Jorissen A., 2010, A&A, 509, 93
Mazur B., Krzeminski W., Kaluzny J., 1995, MNRAS, 273, 59
Mermilliod J. C., Mayor M., Udry S., 2008, A&A, 485, 303
Mikolaitis S., Tautvaišiene G., Gratton R., Bragaglia A., Carreta E., 2012, A&A, 541, A137
Mishenina T. V., Soubiran C., Kovtyukh V. V., Korotin S. A., 2004, A&A, 418, 551
Mishenina T., Korotin S., Carraro G., Kovtyukh V. V., Yegorova I. A., 2013a, MNRAS, 433, 1436

Mishenina T. V., Pignatari M., Korotin S. A., Soubiran C., Charbonnel C., Thielemann F.-K., Gorbaneva T. I., Basak N. Yu., 2013b, A&A, 552, A128
Mishenina T., Kovtyukh V. V., Korotin S., Yegorova I. A., Carraro G., 2014, Mem. Soc. Astron. Ital., 85, 295
Mocak M., Siess L., Muller E., 2011, A&A, 533, 53
Monaco L. et al., 2014, A&A, 564, L6
Montes F. et al., 2007, ApJ, 671, 1685
Nomoto K., Kobayashi C., Tominaga N., 2013, ARA&A, 51, 457
Pace G., Danziger J., Carraro G., Melendez J., Francois P., Matteucci F., Santos N. C., 2010, A&A, 515, A28
Pancino E., Carrera R., Rossetti E., Gallart C., 2010, A&A, 511, A56
Pignatari M., Gallino R., Meynet G., Hirschi R., Herwig F., Wiescher M., 2008, ApJ, 687, 95
Qian Y.-Z., Wasserburg G. J., 2008, ApJ, 687, 272
Reddy A. B. S., Giridhar S., Lambert D. L., 2012, MNRAS, 419, 1350
Reddy A. B. S., Giridhar S., Lambert D. L., 2013, MNRAS, 431, 3338
Rutten R. J., 1978, Sol. Phys., 56, 237
Santos N. C., Lovis C., Pace G., Melendez J., Naef D., 2009, A&A, 493, 309
Sestito P., Bragaglia A., Randich S., Pallavicini R., Andrievsky S. M., Korotin S. A., 2008, A&A, 488, 943
Smiljanic R., Gauderon R., North P., Barbuy B., Charbonnel C., Mowlavi N., 2009, A&A, 502, 267
Stancliffe R. J., Dearborn D., Lattanzio J., Heap S., Campbell S. W., 2011, ApJ, 742, 121
Thielemann F.-K. et al., 2011, Prog. Part. Nucl. Phys., 66, 346
Timmes F. X., Brown E. F., Truran J. W., 2003, ApJ, 590, 83
Travaglio C., Gallino R., Arnone E., Cowan J., Jordan F., Sneden Ch., 2004, ApJ, 601, 864
Travaglio C., Hillebrandt W., Reinecke M., 2005, A&A, 443, 1007
Trippella O., Busso M., Maiorca E., Käppeler F., Palmerini S., 2014, ApJ, 787, 11
Tsymbal V. V., 1996, in Adelman S. J., Kupka F., Weiss W. W., eds, ASP Conf. Ser. Vol. 108, M.A.S.S.; Model Atmospheres and Spectrum Synthesis. Astron. Soc. Pac., San Francisco, p. 198
Woodward P. R., Herwig F., Lin P.-H., 2013, preprint (arXiv:1307.3821)
Yong D., Carney B. W., Teixera de Almeida M.-L., 2005, AJ, 130
Yong D., Carney B. W., Friel E., 2012, AJ, 144, 95

This paper has been typeset from a TEX/LATEX file prepared by the author.